

An Integrodifferential Equation Modeling 1-D Swarming Behavior

Andrew Leverentz

Andrew Bernoff, Advisor

Chad Topaz, Reader

May, 2008

HARVEY MUDD
COLLEGE

Department of Mathematics

Copyright © 2008 Andrew Leverentz.

The author grants Harvey Mudd College the nonexclusive right to make this work available for noncommercial, educational purposes, provided that this copyright statement appears on the reproduced materials and notice is given that the copying is by permission of the author. To disseminate otherwise or to republish requires written permission from the author.

Abstract

We explore the behavior of an integrodifferential equation used to model one-dimensional biological swarms. In this model, we assume the motion of the swarm is determined by pairwise interactions, which in a continuous setting corresponds to a convolution of the swarm density with a pairwise interaction kernel. For a large class of interaction kernels, we derive conditions that lead to solutions which spread, blow up, or reach a steady state. For a smaller class of interaction kernels, we are able to make more quantitative predictions. In the spreading case, we predict the approximate shape and scaling of a similarity profile, as well as the approximate behavior at the endpoints of the swarm (via solutions to a traveling-wave problem). In the blow-up case, we derive an upper bound for the time to blow-up. In the steady-state case, we use previous results to predict the equilibrium swarm density. We support our predictions with numerical simulations.

We also consider an extension of the original model which incorporates external forces. By analyzing and simulating particular cases, we determine that the addition of an external force can qualitatively change the behavior of the system.

Contents

Abstract	iii
Acknowledgments	ix
1 Introduction	1
1.1 Literature Review	2
1.2 A Brief Overview	3
2 Basic Properties of the Model	5
2.1 Conservation of Mass	5
2.2 Conservation of Center of Mass	5
3 Asymptotic Behavior of Solutions	7
3.1 Long-Wave Behavior	9
3.2 Short-Wave Behavior	11
3.3 Predicting Qualitative Behavior	12
4 Spreading Solutions	15
5 Contracting Solutions	23
6 Steady-State Solutions	27
7 Introducing an External Force	29
8 Attractive Swarms in Repulsive Potentials	31
8.1 A Simple Example	31
8.2 General Repulsive Potentials	32
8.3 Physically Relevant Scenarios	35

9	Repulsive Swarms in Attractive Potentials	37
9.1	Necessary Conditions for Steady-State Solutions	37
9.2	Finite-Capacity and Infinite-Capacity Potentials	39
9.3	Example I: An Infinite-Capacity Potential	39
9.4	Example II: A Finite-Capacity Potential	40
9.5	Example III: Looking for an Unusual Potential	49
10	Conclusions and Future Work	53
A	Numerical Methods	55
A.1	Discrete Swarming Model	55
A.2	The Numerical Algorithm	55
A.3	Convergence	56
	Bibliography	59

List of Figures

3.1	Sample asymptotic behaviors	8
3.2	Testing predictions of asymptotic behavior	14
4.1	Spreading swarm approaching Barenblatt similarity solution	16
4.2	RMS width of spreading swarm	17
4.3	Endpoint behavior of spreading solution	21
5.1	Time to blow-up compared to analytic upper bound	25
6.1	Steady-state in agreement with predictions	28
8.1	Simple attractive swarm in repulsive potential	33
8.2	More complex attractive swarm in repulsive potential	35
8.3	Attractive swarm in physically relevant repulsive potential	36
9.1	Repulsive swarm in infinite-capacity attractive potential approaching steady-state	41
9.2	Family of steady-states for repulsive swarm in infinite-capacity attractive potential	42
9.3	Function μ_Q associated with finite-capacity potential	43
9.4	Steady-state solutions associated with finite-capacity potential	44
9.5	Behavior of excess-mass initial condition in finite-capacity potential	46
9.6	Spreading excess-mass solutions matched with half-parabolas	47
9.7	Dependence on width of initial condition in finite-capacity potential	48
9.8	Functions describing infinite-capacity potential with unusual behavior	51
9.9	Unusual behavior in steady-states	52

Acknowledgments

I would like to thank my research advisors, Andrew Bernoff (HMC) and Chad Topaz (Macalester), for their patience, advice, and support.

A previous draft of this thesis was adapted and submitted to a research journal for publication. Professors Bernoff and Topaz made many helpful changes and additions to that draft, some of which have found their way into this latest revision.

Chapter 1

Introduction

Many biological organisms, including fish, birds, insects, and herd animals, form socially cohesive aggregates and exhibit swarming behavior. There exist many previously-published mathematical models for biological swarming; for example, see [1, 4, 6, 7, 8, 9, 12].

As outlined in the work of Mogilner et al. [9], such models can be categorized according to several of their key mathematical properties. A model can describe swarming systems that reside in domains of one, two, or three dimensions. Models may also differ in their treatment of the individuals' interactions with each other and with their environment. Generally speaking, aggregation is governed by endogenous and exogenous forces. Endogenous forces may include pairwise social-interaction forces such as attraction and repulsion, and exogenous forces may include gravity, wind, and chemotaxis. Different models may incorporate different types of forces and may neglect others. Even when considering a particular type of force, models may differ in how they describe that particular force mathematically. For example, as we will see below, in models that describe social interactions by assigning an interaction strength to every possible distance of separation, there is an infinite space of functions to choose from. Moreover, models may be either kinematic or dynamic. Dynamic models utilize Newton's third law and incorporate the effects of inertia upon acceleration, whereas kinematic models neglect inertial forces and assume that a particle's velocity is always proportional and parallel to the net force it experiences. Finally, a model may be discrete or continuous. Continuous models describe a swarm in terms of a continuous density function, and discrete models track the positions of a finite number of localized individuals.

In this thesis, we characterize and quantify the behavior of a class of

swarming models that incorporate pairwise social interactions and allow for the possibility of external forces. We consider a one-dimensional, continuous, kinematic swarming model governed by the following integrodifferential equation:

$$\rho_t + (\rho v)_x = 0, \quad (1.1)$$

$$v(x, t) = \int_{-\infty}^{\infty} \rho(z, t) F_s(x - z) dz + F_c(x). \quad (1.2)$$

Here, $\rho(x, t)$ denotes the swarm density at position x and time t . The function F_s describes a pairwise social-interaction force, and F_c describes an external force, such as gravity or chemotaxis. We note that (1.1) is formulated as a local conservation law. Equation (1.2) describes the swarm's velocity as a continuous superposition of pairwise interactions.

The function F_s specifies a strength of interaction between two clumps of density for any given distance of separation. We assume that F_s is antisymmetric to ensure that distinct clumps of density exert equal and opposite forces on one another. Also, we assume that $F_s(r) \rightarrow 0$ as $r \rightarrow \pm\infty$ in order to model the limited range of interaction exhibited by biological organisms. Finally, to simplify our analysis, we will assume that F_s is continuous and differentiable everywhere, except possibly at the origin, where we allow a jump discontinuity. One reasonable choice of F_s is the Morse interaction force, given by

$$F_s(r) = \text{sgn}(r) \left[-F e^{-|r|/L} + e^{-|r|} \right], \quad (1.3)$$

where F and L are constant parameters specifying the relative strength and length-scale, respectively, of the attractive term relative to the repulsive. While many of our derivations below apply to arbitrary F_s , using this particular interaction force often simplifies the calculations greatly.

The function F_c specifies the strength of the external force experienced by the swarm at a given position. We will consider only functions F_c that are antisymmetric about the origin. Our analysis begins by assuming that there is no external force (i.e., $F_c \equiv 0$). After characterizing the behavior of the simplified system, we introduce non-trivial external forces, such as $F_c(x) = e^{-x^2}$ or $F_c(x) = x^2$.

1.1 Literature Review

Others have studied similar models. For example, Bodnar and Velazquez in [3] and [4] study a continuous, 1-dimensional swarming model using a

rigorous functional analysis framework. In the first paper, they derive the continuous governing equation from a discrete, individual-based model. In the second, they predict that the long-wave components of the density behave according to the porous medium equation, and that the short-wave components behave according to Burgers' equation. From this, they derive conditions on blow-up and spreading.

Bernoff and Topaz, in [1], use a calculus-of-variations argument to find the equilibrium states, when they exist, for a continuous, 1-d model similar to ours. Additionally, they allow for both exogenous and endogenous forces.

Bertozzi and Laurent, in [2], consider a higher-dimensional analogue of the model considered in this paper, and derive conditions that ensure the density will blow up.

Topaz, Bertozzi, and Lewis, in [14], study a higher-dimensional generalization of our model and study its transient "clumping" and "coarsening" behavior.

Mogilner and Edelstein-Keshet, in [8], study a 1-D continuous model similar to ours (where the velocity is a convolution of the density and an interaction force) and look for cohesive "traveling-band" solutions. They find that a non-local model (in which the velocity term $v(x, t)$ depends on the density at locations other than x) is better able to encapsulate cohesive swarm motion than local models.

Topaz and Bertozzi, in [13], study a continuous, 2-dimensional, non-local swarming model and derive predictions about the evolution of the shape of a swarm, including whether swarms will contract or expand and whether they will form spiral-like structures.

1.2 A Brief Overview

In what follows, we initially assume $F_c \equiv 0$ and predict the asymptotic behavior of the system for various interaction forces F_s , making quantitative predictions about the evolution of the swarm density for each observed class of behavior. Then, we extend the model by incorporating a non-trivial external force F_c and study the effect this has on the system's qualitative behavior. Chapters 2 through 6 discuss the simplified model in which $F_c \equiv 0$, and Chapters 7 through 9 discuss the addition of a non-trivial external force.

Chapter 2

Basic Properties of the Model

In this chapter, we prove some basic properties about the simplified model in which $F_c \equiv 0$. Hence, the relevant governing equations are

$$\rho_t + (\rho v)_x = 0, \quad (2.1)$$

$$v(x, t) = \int_{-\infty}^{\infty} \rho(z, t) F_s(x - z) dz. \quad (2.2)$$

2.1 Conservation of Mass

In general, the continuous system conserves mass, which follows from the fact that the governing equation (2.1) is formulated as a conservation law. If we define the mass of the system at time t to be

$$M(t) = \int_{-\infty}^{\infty} \rho(x, t) dx, \quad (2.3)$$

we see that

$$\frac{dM}{dt} = \int_{-\infty}^{\infty} \rho_t dx = - \int_{-\infty}^{\infty} (\rho v)_x dx = - [\rho v]_{x=-\infty}^{x=+\infty} = 0, \quad (2.4)$$

assuming the density decays to zero as $x \rightarrow \pm\infty$. Hence, it makes sense to define $M \equiv M(0) = M(t)$, representing the mass of the system at any time.

2.2 Conservation of Center of Mass

Physically, the antisymmetry of the social interaction force F_s corresponds to interactions occurring in pairs of equal magnitude and opposite direc-

6 Basic Properties of the Model

tion. This suggests intuitively that the center of the mass of the system should remain fixed.

To verify this, we consider the center of mass at time t :

$$\bar{x}(t) = \frac{1}{M} \int_{-\infty}^{\infty} x \rho(x, t) dx. \quad (2.5)$$

Then,

$$\begin{aligned} \frac{d\bar{x}}{dt} &= \frac{1}{M} \int_{-\infty}^{\infty} x \rho_t dx \\ &= -\frac{1}{M} \int_{-\infty}^{\infty} x (\rho v)_x dx \\ &= -\frac{1}{M} [x \rho v]_{x=-\infty}^{x=+\infty} + \frac{1}{M} \int_{-\infty}^{\infty} \rho v dx. \end{aligned} \quad (2.6)$$

Assuming the density vanishes at $\pm\infty$,

$$\begin{aligned} \frac{d\bar{x}}{dt} &= \frac{1}{M} \int_{-\infty}^{\infty} \rho v dx \\ &= \frac{1}{M} \int_{-\infty}^{\infty} \rho(x, t) \int_{-\infty}^{\infty} \rho(y, t) F_s(x - y) dy dx \\ &= \frac{1}{M} \int_{-\infty}^{\infty} \int_{-\infty}^{\infty} \rho(x, t) \rho(y, t) F_s(x - y) dy dx \end{aligned} \quad (2.7)$$

Relabeling the variables of integration and invoking the antisymmetry of the social interaction force,

$$\begin{aligned} \frac{d\bar{x}}{dt} &= \frac{1}{M} \int_{-\infty}^{\infty} \int_{-\infty}^{\infty} \rho(y, t) \rho(x, t) F_s(y - x) dx dy \\ &= -\frac{1}{M} \int_{-\infty}^{\infty} \int_{-\infty}^{\infty} \rho(x, t) \rho(y, t) F_s(x - y) dy dx \end{aligned}$$

Hence, $d\bar{x}/dt = -d\bar{x}/dt$, and thus $d\bar{x}/dt = 0$. That is, the center of mass is stationary.

Chapter 3

Asymptotic Behavior of Solutions

In this chapter, we discuss observed classes of asymptotic behavior for the simplified system in which $F_c \equiv 0$ and propose conditions on the social force F_s leading to each class of behavior. The relevant governing equations are

$$\rho_t + (\rho v)_x = 0, \quad (3.1)$$

$$v(x, t) = \int_{-\infty}^{\infty} \rho(z, t) F_s(x - z) dz. \quad (3.2)$$

To simulate this system, we used a particle-based numerical method, which is described in the appendix. Furthermore, we assumed a Morse-type social interaction force of the form (1.3). Simulations revealed three asymptotic behaviors, namely spreading, steady-state, and blow-up. These behaviors are shown in Figure 3.1. Figure 3.1(a) shows a spreading solution, corresponding to a population that disperses to infinity. The population density profiles appear to be self-similar; we discuss this issue further in Chapter 4. Figure 3.1(b) shows a steady-state solution, corresponding to an localized aggregation of the population. The population density drops discontinuously to 0 at the edge of the support. Figures 3.1(c,d) show two cases of solutions blow-up, corresponding to over-crowded populations. In the first case, the solution forms a single clump. In the second case, multiple, mutually-repelling clumps form. These clumps are, in fact, delta functions, as we discuss later.

In what follows, we derive conditions on the social force F_s that should produce each of the above behaviors. To do this, we examine long-wave and short-wave behavior separately.

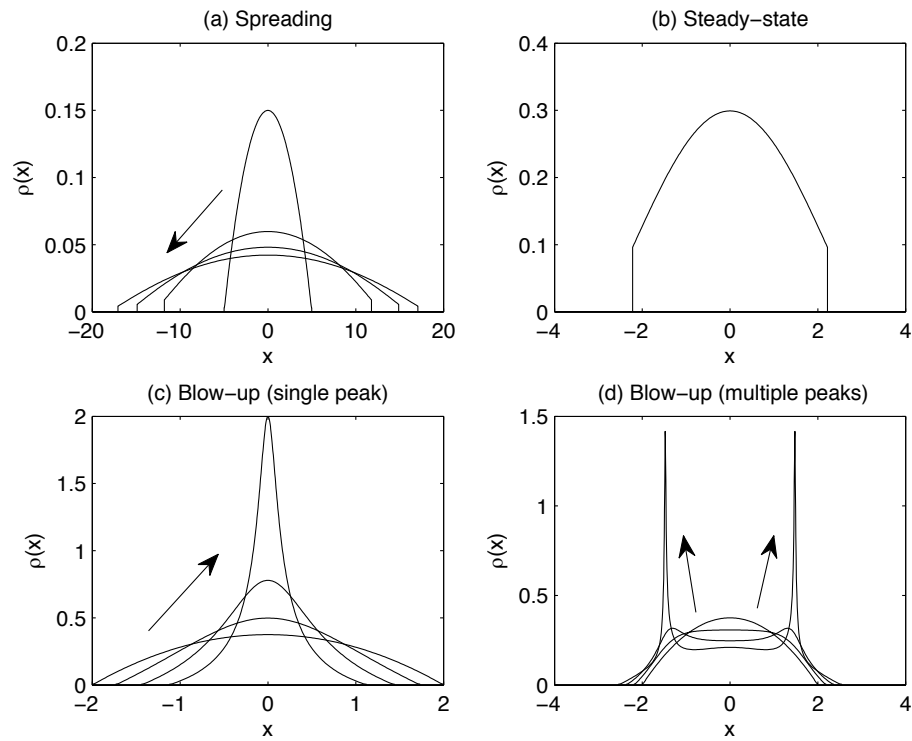


Figure 3.1: Snapshots of the population density profile governed by (3.1) with the social interactions described by the Morse interaction force (1.3). The asymptotic behavior of the model depends crucially on the choice of F , the relative strength of social attraction to social repulsion, and L , their relative characteristic length scales. (a) $F = 0.1$, $L = 2$. The population eventually spreads to infinity. (b) $F = 0.5$, $L = 3$. The population reaches a compactly-supported steady state. (c) $F = 2$, $L = 2$. The density profile blows up into a single clump. (d) $F = 2$, $L = 0.5$. The density profile blows up by forming mutually-repulsive clumps.

3.1 Long-Wave Behavior

In this section, we predict what happens to wide and slowly-varying (i.e., “long-wave”) initial conditions, finding that they behave, for small time, according to a porous-medium equation.

We first note that the Fourier transform of the velocity $v(x, t)$ is given by a product of Fourier transforms, since v is in the form of a convolution:

$$\hat{v}(k) = \mathcal{F}\{\rho * F_s\} = \hat{\rho}(k)\hat{F}_s(k). \quad (3.3)$$

If we assume that ρ is initially long-wave, meaning $\hat{\rho}$ is localized near $k = 0$, we can eventually ignore the behavior of \hat{F}_s for large k . We begin by writing $\hat{F}_s(k)$ as a Taylor series:

$$\hat{v}(k) = \hat{\rho}(k) \sum_{n=0}^{\infty} \frac{k^n}{n!} \hat{F}_s^{(n)}(0). \quad (3.4)$$

Furthermore, we can express the n^{th} derivative of \hat{F}_s at $k = 0$ in terms of the moments of F_s . We define the n^{th} moment of F_s by

$$M_n[F_s] = \int_{-\infty}^{\infty} z^n F_s(z) dz \quad (3.5)$$

Then,

$$\begin{aligned} \hat{F}_s^{(n)}(0) &= \left[\frac{d^n}{dk^n} \int_{-\infty}^{\infty} F_s(x) e^{-ikx} dx \right]_{k=0} \\ &= \left[\int_{-\infty}^{\infty} F_s(x) \frac{d^n}{dk^n} e^{-ikx} dx \right]_{k=0} \\ &= (-i)^n \left[\int_{-\infty}^{\infty} x^n F_s(x) e^{-ikx} dx \right]_{k=0} \\ &= (-i)^n \int_{-\infty}^{\infty} x^n F_s(x) dx \\ &= (-i)^n M_n[F_s]. \end{aligned} \quad (3.6)$$

From this,

$$\begin{aligned} \hat{v}(k) &= \sum_{n=0}^{\infty} \frac{(-1)^n}{n!} (ik)^n \hat{\rho}(k) M_n[F_s] \\ &= \sum_{n=0}^{\infty} \frac{(-1)^n}{n!} \mathcal{F} \left\{ \frac{\partial^n \rho}{\partial x^n} \right\} M_n[F_s]. \end{aligned} \quad (3.7)$$

Since F_s is antisymmetric, the even moments of F_s vanish and we can write

$$\hat{v}(k) = - \sum_{n=0}^{\infty} \frac{1}{(2n+1)!} \mathcal{F} \left\{ \frac{\partial^{2n+1} \rho}{\partial x^{2n+1}} \right\} M_{2n+1}[F_s]. \quad (3.8)$$

Under the assumption that ρ is initially long-wave, we can neglect the behavior of $\hat{F}_s(k)$ for large k and truncate this Taylor series:

$$\hat{v}(k) \approx -M_1[F_s] \mathcal{F}\{\rho_x\}. \quad (3.9)$$

Then,

$$v(x) \approx -M_1[F_s] \rho_x. \quad (3.10)$$

With the velocity in this form, the governing equation approaches

$$\rho_t = \kappa(\rho^2)_{xx}, \quad \text{where} \quad \kappa = \frac{1}{2} M_1[F_s]. \quad (3.11)$$

This is the well-known porous-medium equation. For certain initial conditions, a class of similarity solutions known as Barenblatt solutions are given by

$$\rho(x, t) = \frac{1}{12(t+t_0)^{1/3}} \left[a_0^2 - \left(\frac{x-x_0}{(t+t_0)^{1/3}} \right)^2 \right]_+, \quad (3.12)$$

where we use the notation $[u]_+ = \max\{0, u\}$, and where x_0 , t_0 , and a_0 are parameters depending on the initial condition [15]. Additionally, all initial conditions will approach this particular class of solutions asymptotically as $t \rightarrow \infty$.

For $\kappa > 0$, solutions to this equation spread and grow wider without bound. For $\kappa < 0$, the porous-medium equation models backwards diffusion, which means that solutions will contract and blow up rather than spread.

Thus, when $\kappa > 0$, long-wave initial conditions will lead to solutions of (3.1) that spread and grow wider without bound. This is asymptotically consistent; that is, long-wave solutions will spread and therefore remain long-wave when $\kappa > 0$. However, when $\kappa < 0$, long-wave initial conditions will contract until they can no longer be considered long-wave, at which point the approximations used above will fail to hold.

Finally, we note that if $\kappa = 0$ (that is, if the first moment of F_s vanishes), the above analysis does not hold, and we must retain higher-order terms in (3.8) in order to predict asymptotic behavior.

3.2 Short-Wave Behavior

In this section, we predict what happens to narrow and sharply-varying (i.e., “short-wave”) initial conditions, finding that they behave according to Burgers’ equation, at least for a short time.

We assume ρ is initially short-wave. This will eventually allow us to neglect the behavior of $\hat{F}_s(k)$ near $k = 0$.

We begin by writing the governing equation in terms of the following cumulative mass function:

$$\psi(x, t) = \int_{\bar{x}}^x \rho(z, t) dz. \quad (3.13)$$

Here, \bar{x} is the center of mass of the system. We recall that this is constant with respect to time provided F_s is antisymmetric, as discussed above.

We can write the governing equation as:

$$\begin{aligned} \psi_t(x, t) &= \int_{\bar{x}}^x \rho_t(z, t) dz \\ &= - \int_{\bar{x}}^x (\rho(z, t)v(z, t))_x dz \\ &= -\rho(x, t)v(x, t) \\ &= -\psi_x(x, t)v(x, t). \end{aligned} \quad (3.14)$$

That is, the cumulative mass function behaves according to

$$\psi_t + v\psi_x = 0. \quad (3.15)$$

If F_s is smooth everywhere except for a jump discontinuity in its m th derivative at the origin—that is, if $F_s^{(m+1)}(x) = 2\beta\delta(x) + S(x)$ for $\beta \neq 0$ and S continuous and piecewise differentiable—we can use repeated integration by parts to obtain

$$\begin{aligned} \hat{F}_s(k) &= \int_{-\infty}^{\infty} F_s(x)e^{-ikx} dx \\ &= \frac{1}{(ik)^{m+1}} \int_{-\infty}^{\infty} F_s^{(m+1)}(x)e^{-ikx} dx \\ &= \frac{1}{(ik)^{m+1}} [2\beta + \hat{S}(k)]. \end{aligned} \quad (3.16)$$

Since S is smooth, the Riemann-Lebesgue lemma states that its Fourier transform goes to zero as $k \rightarrow \infty$. If ρ is initially short-wave, then we can

focus solely on the behavior of $\hat{F}_s(k)$ as $k \rightarrow \infty$:

$$\hat{F}_s(k) \sim \frac{2\beta}{(ik)^{m+1}} \quad \text{as } k \rightarrow \infty. \quad (3.17)$$

We commonly deal with interaction forces where the jump discontinuity occurs at the origin in the function F_s itself, in which case $m = 0$ and

$$\hat{F}_s(k) \sim \frac{2\beta}{ik} \quad \text{as } k \rightarrow \infty. \quad (3.18)$$

Therefore, in this limit, the velocity becomes

$$\hat{v}(k) \sim \frac{2\beta}{ik} \hat{\rho}(k) \quad \text{as } k \rightarrow \infty. \quad (3.19)$$

Since $\psi_x = \rho$, we have $\hat{\rho}(k) = ik\hat{\psi}(k)$ and thus

$$v \approx 2\beta\psi \quad \text{in the limit of short wavelengths.} \quad (3.20)$$

Hence, the governing equation for the cumulative mass function ψ reduces to Burgers' equation:

$$\psi_t + 2\beta\psi\psi_x = 0. \quad (3.21)$$

Since ψ is always monotonically increasing, we know that it will contract and form a shock when $\beta < 0$ and spread when $\beta > 0$. Moreover, because $\psi_x = \rho$, we predict that ρ will blow up when $\beta < 0$ and spread when $\beta > 0$.

The above approximations are asymptotically consistent for $\beta < 0$ (since narrow initial conditions will become narrower), but asymptotically inconsistent for $\beta > 0$. In the latter case, narrow initial conditions will spread until they can no longer be considered narrow.

When $\beta = 0$, we know that F_s itself is continuous, and therefore $m \geq 1$ in (3.17). Hence, our approximation for the governing equation may involve antiderivatives of the cumulative mass function ψ .

3.3 Predicting Qualitative Behavior

From the above results, we expect short waves to blow up when $\beta < 0$ and spread when $\beta > 0$. Similarly, we expect long waves to contract when $\kappa < 0$ and spread when $\kappa > 0$. When short waves blow up, we expect the short-wave instability to override the long-wave behavior. Thus, there are three possible cases:

- Solutions contract when $\beta < 0$, regardless of the value of κ , leading to blow-up.
- When $\beta > 0$ and $\kappa > 0$, both long and short waves spread.
- When $\beta > 0$ and $\kappa < 0$, short waves spread while long waves contract, tending toward an equilibrium solution.

To test these predictions, we have performed numerical simulations of (3.1) with social interactions given by the Morse potential (1.3). For this choice of potential, $\kappa = 1 - FL^2$ and $\beta = 1 - F$. Thus, we expect to see blow up when $F > 1$, spreading when $F < 1/L^2$ and $F < 1$, and steady-state solutions when $1 > F > 1/L^2$. The results of the numerical simulations are summarized in Figure 3.2, which shows that the boundaries between the three regimes agree with our theoretical predictions.

When $F > 1$, the numerical solution consistently blows up, but we observe two distinct types of blow-up. When $L < 1$, the interaction force F_s models long-range repulsion, and the solution may form multiple δ -functions which travel away from each other, whereas when $L > 1$, the entire mass of the system eventually collapses into a single δ -function due to long-range attraction.

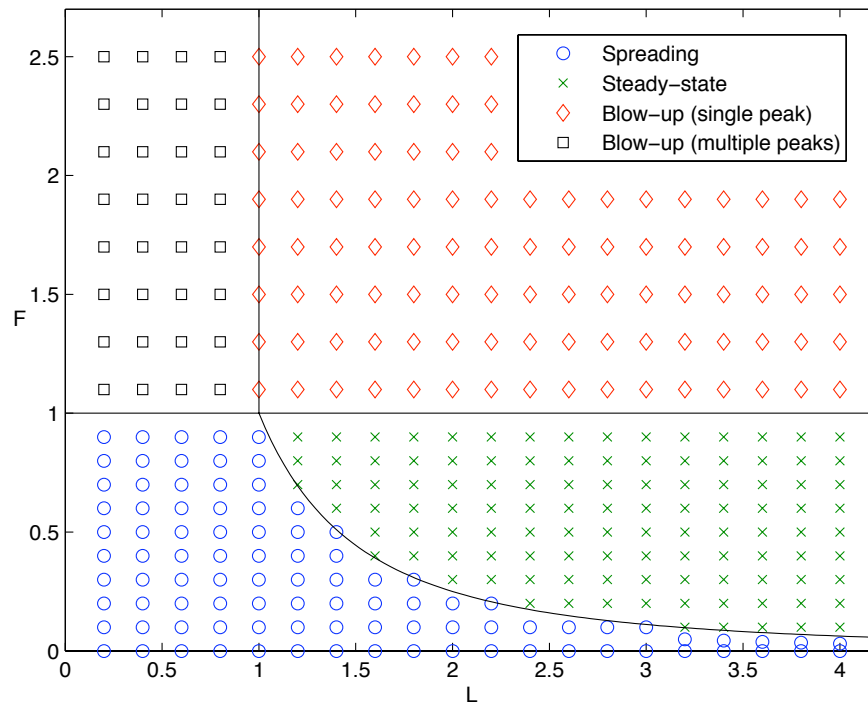


Figure 3.2: Results of numerical simulations of (3.1) with the Morse-type social interaction (1.3). The horizontal line at $F = 1$ corresponds to $\beta = 0$ and marks the boundary above which solutions blow up. The curve $F = 1/L^2$ corresponds to $\kappa = 0$ and marks the boundary between spreading and steady state solutions for $F < 1$. The (partial) line $L = 1$ indicates the critical case separating whether attraction operates at short or long ranges. When in the blow-up (strong attraction) regime, this boundary marks where a transition between different types of blow-up occur. When the attraction is short range, multiple repelling delta-functions form. When the attraction is long range, a single delta function forms.

Chapter 4

Spreading Solutions

Still in the context of the simplified model (where $F_c \equiv 0$), we now consider particular cases where the predictions of the preceding chapter lead us to expect swarms to spread indefinitely.

When $\kappa > 0$ and $\beta > 0$, we expect solutions to spread. As the density profile grows wider, the long-wave approximation derived above will become increasingly accurate, and so we expect solutions to approach Barenblatt's solution to the porous-medium equation, which is given in (3.12).

As shown in Figures 4.1 and 4.2, numerical results using a Morse interaction force (with $F < 1$ and $F < 1/L^2$) produced spreading solutions that agree with the Barenblatt solution.

Apart from the shape of the solution, we are also interested in studying the jump discontinuities at the edges of the swarm.

When we assume a Morse-type social interaction force, we can gain a more quantitative understanding of this endpoint behavior by finding an exact traveling-wave solution to (3.1). At the left endpoint of the swarm, for example, we might expect a spreading solution to behave locally (and for small t) like a fixed wave profile traveling to the left. Hence, we look for a traveling-wave solution of the form $\rho(x, t) = g(x + ct)$, where $g(z) = 0$ for all $z < 0$.

Under these assumptions, the PDE reduces to

$$0 = cg' + \frac{\partial}{\partial z}(vg) = \frac{\partial}{\partial z}[(c + v)g]. \quad (4.1)$$

Integrating both sides of this equation,

$$(c + v)g = 0. \quad (4.2)$$

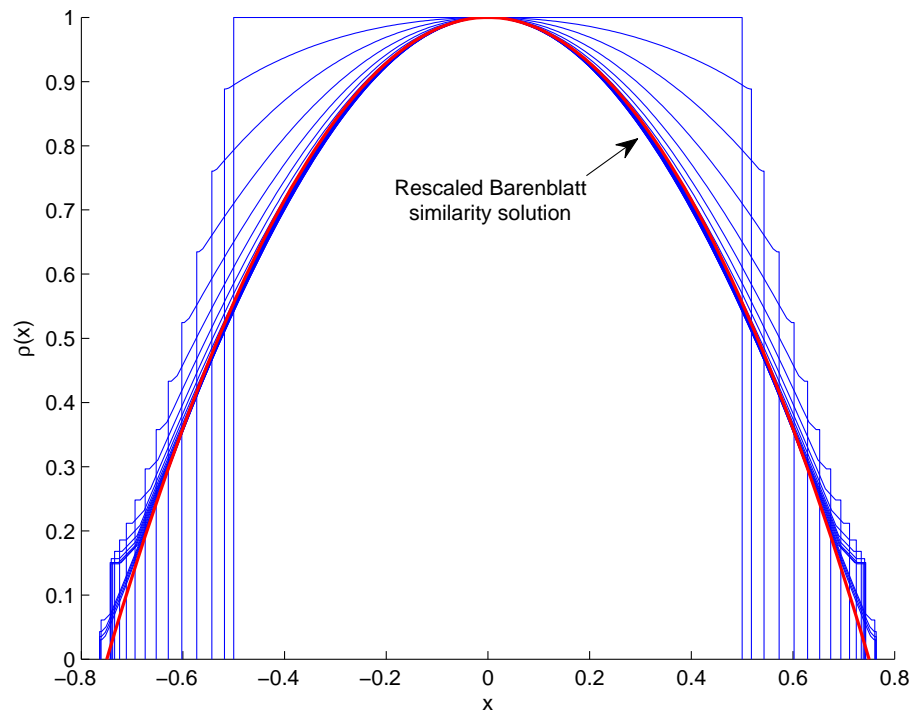


Figure 4.1: In the spreading regime, we see that the density profile, if properly rescaled, approaches the Barenblatt similarity solution to the porous-medium equation. To visualize this convergence, we have normalized the numerical results by maximum height. A representative snapshot of the Barenblatt similarity solution is shown for comparison. For this simulation, we used a Morse interaction force with parameters $F = 0.2$ and $L = 2$.

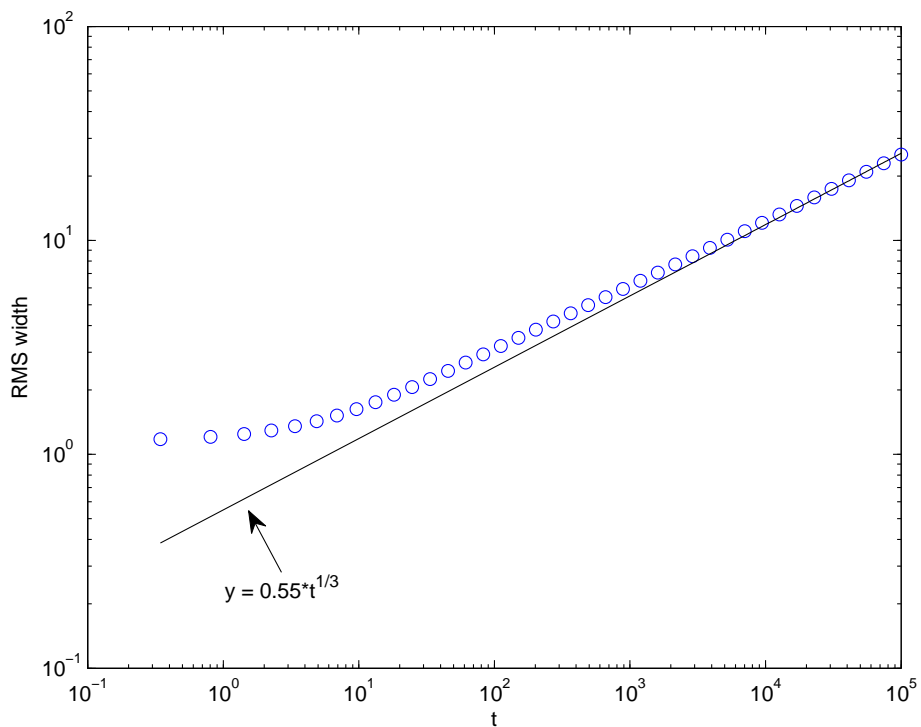


Figure 4.2: In the spreading regime, this plot shows that the RMS width of the density profile grows approximately according to a power law with exponent $1/3$, matching the behavior of the Barenblatt similarity solution to the porous-medium equation. As in Figure 4.1, this simulation used a Morse interaction force with parameters $F = 0.2$ and $L = 2$.

We know that the constant of integration must be zero because the left-hand side vanishes for negative z . Hence, wherever g is nonzero, $c = -v$. That is,

$$-c = \int_0^\infty g(\tilde{z})F_s(z - \tilde{z}) d\tilde{z} \quad \text{for } z \geq 0 \quad (4.3)$$

After writing out F_s explicitly and taking derivatives with respect to z on both sides, we obtain

$$\begin{aligned} 0 = & 2(1-F)g(z) - \int_0^z g(\tilde{z})e^{\tilde{z}-z} d\tilde{z} - \int_z^\infty g(\tilde{z})e^{z-\tilde{z}} d\tilde{z} \\ & + \frac{F}{L} \int_0^z g(\tilde{z})e^{(\tilde{z}-z)/L} d\tilde{z} + \frac{F}{L} \int_z^\infty g(\tilde{z})e^{(z-\tilde{z})/L} d\tilde{z}. \end{aligned} \quad (4.4)$$

That is,

$$(F-1)g(z) = \frac{1}{2} \int_0^\infty g(\tilde{z}) \left[\frac{F}{L} e^{-|z-\tilde{z}|/L} - e^{-|z-\tilde{z}|} \right] d\tilde{z}. \quad (4.5)$$

To ensure that the exponential terms are linearly independent, we assume $F \neq 0$ and $L \neq 1$. Then, to solve this integral equation, we apply the differential operators $\mathcal{L}_1 = \partial_{zz} - 1$ and $\mathcal{L}_2 = L^2 \partial_{zz} - 1$ to both sides.

The left-hand side becomes

$$\begin{aligned} & \mathcal{L}_1 \mathcal{L}_2 [(F-1)g(z)] \\ & = (F-1)L^2 g''''(z) + (1-F+L^2-FL^2)g''(z) + (F-1)g(z), \end{aligned} \quad (4.6)$$

and the right-hand side becomes

$$\begin{aligned} & \frac{1}{2} \int_0^\infty g(\tilde{z}) \mathcal{L}_1 \mathcal{L}_2 \left[\frac{F}{L} e^{-|z-\tilde{z}|/L} - e^{-|z-\tilde{z}|} \right] d\tilde{z} \\ & = \frac{1}{2} \int_0^\infty g(\tilde{z}) \cdot (-2) \cdot [(F-L^2)\delta''(z-\tilde{z}) + (1-F)\delta(z-\tilde{z})] d\tilde{z} \\ & = (L^2-F)g''(z) + (F-1)g(z). \end{aligned} \quad (4.7)$$

Hence, the integral equation reduces to the following ODE:

$$g''''(z) - \frac{1-FL^2}{L^2(1-F)}g''(z) = 0. \quad (4.8)$$

Assuming the solution is spreading, we know $1-FL^2 = \kappa > 0$ and $1-F = \beta > 0$. This tells us that the coefficient on $g''(z)$ is strictly negative.

Then, letting $\alpha = \frac{1}{L}\sqrt{\frac{1-FL^2}{1-F}}$, and integrating the ODE twice, we have

$$g''(z) - \alpha^2 g(z) = Az + B. \quad (4.9)$$

Since A and B are undetermined constants of integration, we can rescale them and rewrite this ODE as

$$g''(z) - \alpha^2 [g(z) - Az - B] = 0. \quad (4.10)$$

We note that $g(z) = Az + B$ is a particular solution to this equation and that $g_h(z) = Ce^{-\alpha z} + De^{\alpha z}$ is the general solution to the corresponding homogeneous equation. Therefore, the general solution to the inhomogeneous equation is

$$g(z) = Az + B + Ce^{-\alpha z} + De^{\alpha z}. \quad (4.11)$$

The traveling wave cannot grow exponentially as $z \rightarrow \infty$, because that implies non-constant mass flux as the wave translates to the left, so we must set $D = 0$.

Next, we can find A , B , and C by plugging this solution into (4.3):

$$-c = \int_0^\infty (A\tilde{z} + B + Ce^{-\alpha\tilde{z}}) \text{sgn}(z - \tilde{z}) \left(-Fe^{-|z-\tilde{z}|/L} + e^{-|z-\tilde{z}|} \right) d\tilde{z}. \quad (4.12)$$

This simplifies to

$$\begin{aligned} -c &= A \cdot \left[2(FL^2 - 1) - FL^2 e^{-z/L} + e^{-z} \right] \\ &+ B \cdot \left[FL e^{-z/L} - e^{-z} \right] \\ &+ C \cdot \left[\frac{FL}{1 - \alpha L} e^{-z/L} - \frac{1}{1 - \alpha} e^{-z} \right]. \end{aligned} \quad (4.13)$$

Since 1 , $e^{-z/L}$, and e^{-z} are linearly independent, we get the following system of equations by matching like terms:

$$A = \frac{c}{2(1 - FL^2)}, \quad (4.14)$$

$$A = B + \frac{C}{1 - \alpha}, \quad (4.15)$$

$$AL = B + \frac{C}{1 - \alpha L}. \quad (4.16)$$

Solving for the coefficients:

$$A = cA_0, \quad A_0 = \frac{1}{2(1 - FL^2)}, \quad (4.17)$$

$$B = cB_0, \quad B_0 = \frac{1}{2(1 - FL^2)} \left(L + 1 - \frac{1}{\alpha} \right), \quad (4.18)$$

$$C = cC_0, \quad C_0 = \frac{1}{2(1 - FL^2)} (\alpha L - 1) \left(1 - \frac{1}{\alpha} \right). \quad (4.19)$$

Note that this gives us a traveling-wave solution for each wave speed c .

From this, we can predict the relationship between the instantaneous speed of a traveling front, the size of the jump at the edge, and the slope of the density at the edge.

In particular, the size of the jump is given by

$$g(0) = (B_0 + C_0)c, \quad (4.20)$$

and the slope at the edge is given by

$$g'(0) = A_0c - \alpha C_0ce^{-\alpha z} \Big|_{z=0} = (A_0 - \alpha C_0)c, \quad (4.21)$$

where the wave speed c is the instantaneous speed of the traveling discontinuity.

Note, however, that we can only expect these relations to hold in the limit as $t \rightarrow \infty$, since the solution must be sufficiently wide and slowly varying near the endpoints for it to locally approximate a traveling wave.

For several values of F and L , we tested these predictions by tracking the speed, jump in density, and slope at the endpoints over time. Figure 4.3 shows that the jump in density and slope, if properly rescaled, approach the instantaneous speed as expected.

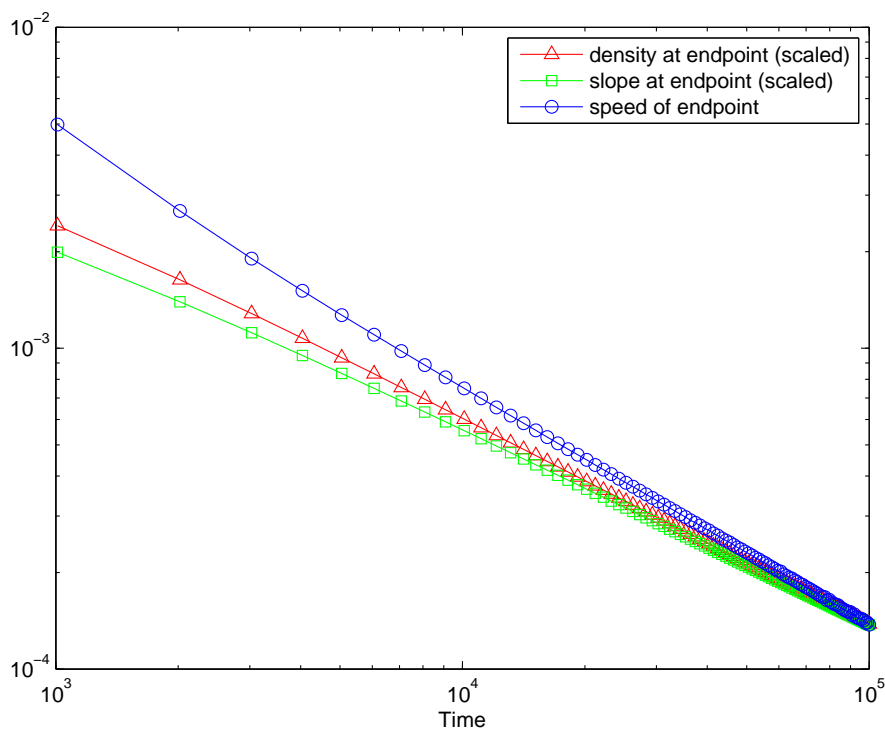


Figure 4.3: The endpoint behavior of a spreading solution matches our traveling-wave predictions. Here, the density at the endpoint is normalized by $B_0 + C_0$, and the slope in density at the endpoint is normalized by $A_0 - \alpha C_0$. We see that these rescaled quantities approach the instantaneous speed of the endpoint, as expected. In this simulation, we used a Morse interaction force with parameters $F = 0.1$ and $L = 3$.

Chapter 5

Contracting Solutions

Now we consider the case where the predictions of Chapter 3 lead us to expect swarms to contract until the swarm density blows up.

When $\beta < 0$ and the initial condition is sufficiently narrow, we can approximately predict when the solution will form a δ -function. We will let $a(t)$ and $b(t)$ denote the position at time t of the left and right endpoints, respectively. Then, for $a(t) < z < b(t)$ and $b(t) - a(t)$ sufficiently small, note that

$$\begin{aligned} F_s(a(t) - z) &\leq \min_{a(t)-b(t) < r < 0} F_s(r) \\ &= \max_{0 < r < b(t)-a(t)} F_s(r) \\ &= \min_{0 < r < b(t)-a(t)} |F_s(r)|. \end{aligned} \tag{5.1}$$

Hence, if we let

$$q(t) = \min_{0 < r < b(t)-a(t)} |F_s(r)|, \tag{5.2}$$

we can find a bound for the velocity at the left endpoint:

$$\begin{aligned} a'(t) &= v(a(t), t) \\ &= \int_{a(t)}^{b(t)} \rho(z, t) F_s(a(t) - z) dz \\ &\geq q(t) \int_{a(t)}^{b(t)} \rho(z, t) dz \\ &= Mq(t) \\ &> 0. \end{aligned} \tag{5.3}$$

A similar argument shows that the velocity at the right endpoint satisfies

$$b'(t) \leq -Mq(t) < 0. \quad (5.4)$$

This demonstrates that the endpoints are approaching each other. Hence, the interval $(0, b(t) - a(t))$ is shrinking. Then, from the definition of $q(t)$, we see that $q(t)$ must be non-decreasing, and consequently the endpoints must be accelerating towards each other, or at least moving towards each other at a constant velocity.

If we let t^* denote the time at which all the mass of the system has entered a single δ -function, we can find an upper bound for t^* using

$$b'(t) \leq b'(0) \leq -Mq(0), \quad (5.5)$$

$$a'(t) \geq a'(0) \geq Mq(0). \quad (5.6)$$

Since the endpoints are initially separated by a distance $b(0) - a(0)$ and are moving towards each other at a minimum speed $Mq(0)$, this gives us the following bound:

$$t^* \leq \frac{b(0) - a(0)}{2Mq(0)}. \quad (5.7)$$

Here we note that Gronwall's inequality might yield a slightly more accurate bound on t^* , but (5.7) should be sufficient for our purposes.

Furthermore, just before the solution forms a δ -function, we can predict that the velocities of the endpoints will be $M|\beta|$ at the left endpoint, and $-M|\beta|$ at the right endpoint. This suggests that when $\beta = 0$ we may have blow-up in infinite time.

Numerical tests of these predictions used narrow initial conditions of widths 0.1 units and 0.2 units, as well as a Morse interaction force satisfying $L > 1$, $F > 1$. For one fixed value of L , Figure 5.1 shows that the upper bound on t^* derived above holds for all tested values of F .

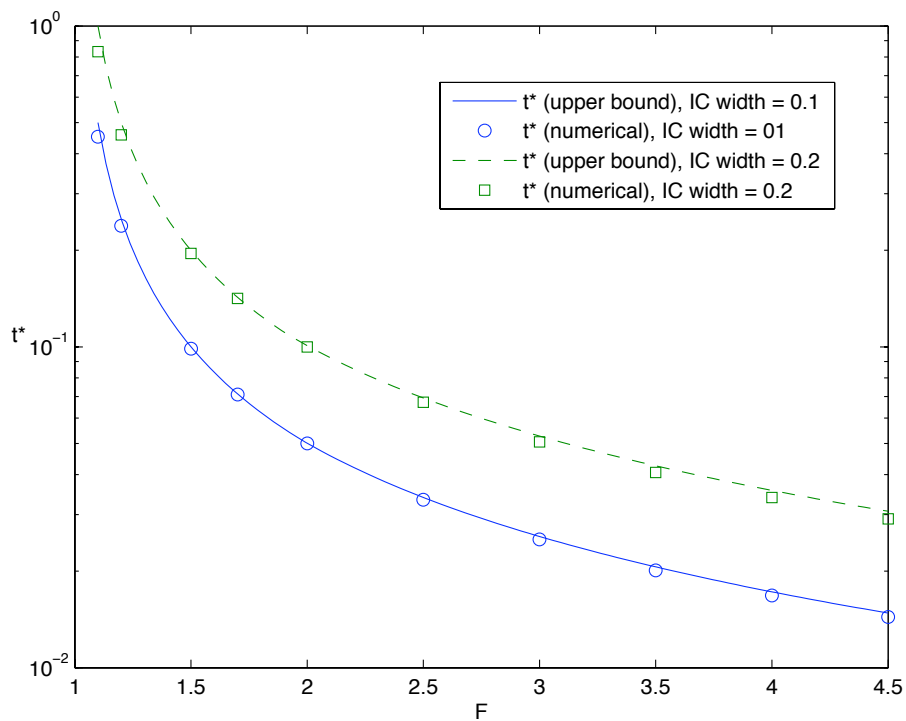


Figure 5.1: Within the blow-up regime, the time to blow-up, t^* , in numerical simulation results compare well with an analytic upper bound for t^* . In these simulations, we tested initial conditions of widths 0.1 units and 0.2 units. We used a Morse interaction force with $L = 2$ and various values for $F > 1$.

Chapter 6

Steady-State Solutions

Next, we consider the case where the results of Chapter 3 predict steady-state solutions.

Assuming a Morse interaction force, the regime in which steady-state solutions are expected corresponds to parameters F and L satisfying $1 > F > 1/L^2$. Looking for steady-state solutions, we assume $\rho_t \equiv 0$. Then, the governing equation (3.1) becomes $(\rho v)_x = 0$. Integrating with respect to x yields $\rho v = 0$. Here, the constant of integration must be zero because swarms of finite support have zero density outside of a sufficiently large radius, and hence ρv is zero for some values of x . Then, wherever $\rho \neq 0$, we have $v = 0$. Using (3.2), this corresponds to the following integral equation:

$$0 = \int_{-\infty}^{\infty} \rho(z) F_s(x-z) dz. \quad (6.1)$$

In the case of a Morse interaction force, the results of [1] allow us to solve this integral equation and thereby predict the equilibrium solution exactly.

Assuming $\kappa = 1 - FL^2 < 0$ and $\beta = 1 - F > 0$, we define the following constants:

$$\mu = \sqrt{\frac{|\kappa|}{L^2\beta}}, \quad (6.2)$$

$$W = \frac{2}{\mu} \tan^{-1} \left(\frac{\sqrt{|\kappa|\beta}}{FL-1} \right), \quad (6.3)$$

$$\lambda = \frac{M}{W + 2(L+1)}, \quad (6.4)$$

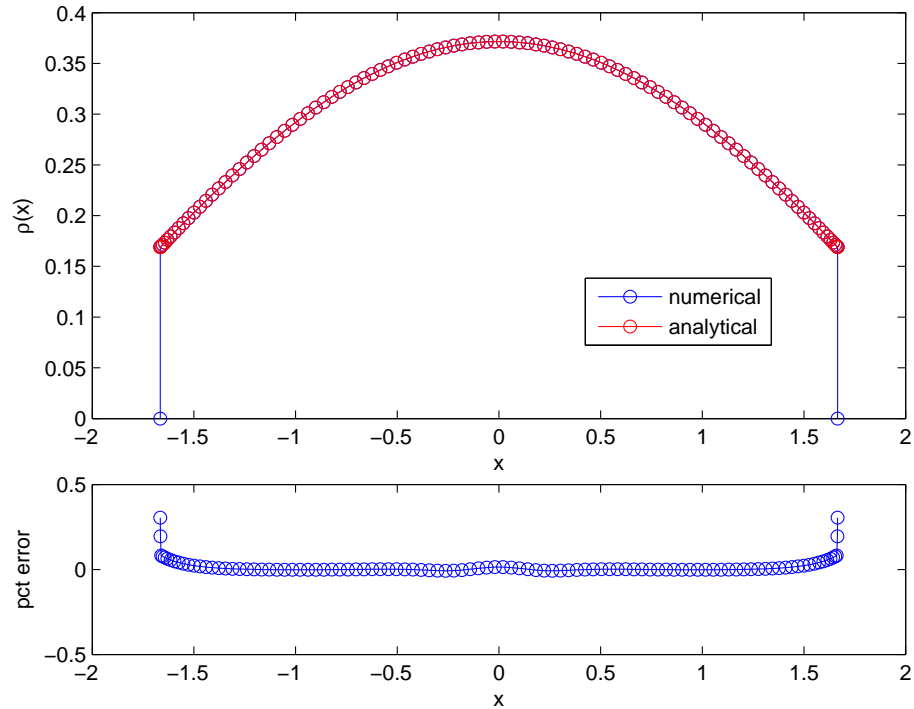


Figure 6.1: In the steady-state regime, the long-term behavior of a numerical simulation agrees well with the predicted equilibrium solution. In this simulation, we used a Morse interaction force with parameters $F = 0.5$ and $L = 2$.

$$A = \frac{\lambda(L^2 - 1)\sqrt{F}}{L\beta}. \quad (6.5)$$

As presented in [1], the equilibrium solution is then

$$\rho(x) = \begin{cases} A \cos(\mu x) + \lambda, & |x| \leq W/2, \\ 0, & |x| > W/2. \end{cases} \quad (6.6)$$

Figure 6.1 shows that our numerical results line up well with these predictions.

Chapter 7

Introducing an External Force

Since swarming behavior is often influenced by environmental factors, we now incorporate an exogenous force $F_c(x)$.¹ With this new force, the governing equations become

$$\rho_t + (\rho v)_x = 0, \quad (7.1)$$

$$v(x, t) = \int_{-\infty}^{\infty} \rho(z, t) F_s(x - z) dz + F_c(x). \quad (7.2)$$

In 1-D, we can associate any force $F_c(x)$ with a corresponding potential $Q(x)$ such that

$$F_c(x) = -Q'(x). \quad (7.3)$$

Hence, we can generally write the velocity $v(x, t)$ as

$$v(x, t) = \int_{-\infty}^{\infty} \rho(z, t) F_s(x - z) dz - Q'(x). \quad (7.4)$$

We assume the potential $Q(x)$ is symmetric (meaning the force $F_c(x)$ must be antisymmetric), continuous, and piecewise smooth. For simplicity, we will consider only forces for which the origin is purely repulsive or purely attractive. Pure repulsion occurs when $Q(x)$ is strictly decreasing for $x > 0$, and pure attraction occurs when $Q(x)$ is strictly increasing for $x > 0$.

Given a social force F_s and an external force F_c , we wish to predict the asymptotic behavior of the system. In particular, we wish to determine when it is possible for the addition of an external force to qualitatively alter the system's asymptotic behavior. In what follows, we do not prove fully

¹Here, the subscript "c" is intended to suggest chemotaxis, although this force could also correspond to gravity, wind advection, or other types of external factors.

general results for arbitrary F_c and F_s ; instead, we consider several particular cases in which it is possible to predict how the addition of an external force will alter the system's behavior.

A brief note on terminology: Throughout this section, we are interested in comparing the behavior of an arbitrary system (with non-trivial F_c) to the corresponding system where $F_c \equiv 0$. We say that an external force F_c (or the associated potential Q) "prevents blow-up" for a given social force F_s if we observe blow-up when the velocity is given by

$$v(x, t) = \int_{-\infty}^{\infty} \rho(z, t) F_s(x - z) dz, \quad (7.5)$$

but not when the velocity is given by

$$v(x, t) = \int_{-\infty}^{\infty} \rho(z, t) F_s(x - z) dz + F_c(x). \quad (7.6)$$

Similarly, we say that F_c "prevents spreading" for a given social force F_s if we observe spreading when the velocity is given by (7.5), but not when the velocity is given by (7.6).

Chapter 8

Attractive Swarms in Repulsive Potentials

We first consider purely attractive social forces F_s , which in the absence of external forces lead to blow-up (as discussed in Chapter 5). In numerical tests, we have observed that the addition of a sufficiently strong repulsive external force can prevent blow-up, leading either to spreading or to an unstable equilibrium. The following analysis determines sufficient conditions for an external force to prevent blow-up.

8.1 A Simple Example

In the simplest case, suppose the social force is $F_s(r) = -\text{sgn}(r)$, and suppose the external potential is $Q(x) = -x^2$, so that $Q'(x) = -2x$.

Assuming the initial density is a constant $\bar{\rho}_0$ for $|x| < b_0$ and zero elsewhere, the initial velocity is given by

$$\begin{aligned} v(x, 0) &= - \int_{-b_0}^{b_0} \bar{\rho}_0 \text{sgn}(x - z) dz + 2x \\ &= \bar{\rho}(b_0 - x) - \bar{\rho}_0(x + b_0) + 2x \\ &= 2(1 - \bar{\rho}_0)x \end{aligned} \tag{8.1}$$

In this particular case, we can use the method of characteristics to find the dynamics of the system at $t = 0$. We find that the characteristics are initially given by

$$x(t) = x_0 e^{2(1 - \bar{\rho}_0)t}, \tag{8.2}$$

with the density initially decaying along these curves according to

$$\rho(x(t), t) = \bar{\rho}_0 e^{-2(1-\bar{\rho}_0)t}. \quad (8.3)$$

Since the expression for ρ does not depend on x , we conclude that piecewise constant initial conditions must remain piecewise constant for all time.

Assuming the initial condition is constant on some interval and zero elsewhere, we let $\bar{\rho}(t)$ denote the nonzero density of the swarm at time t . Using the same argument we used to derive (8.1), we find

$$v(x, t) = 2(1 - \bar{\rho}(t))x. \quad (8.4)$$

Therefore,

$$\frac{\partial}{\partial x} v(x, t) = 2(1 - \bar{\rho}(t)). \quad (8.5)$$

The sign of $\partial v / \partial x$ determines the local behavior of the system. Specifically, the method of characteristics tells us that the density increases (at least locally and for a short time) due to net inward mass flux when $\partial v / \partial x$ is negative; likewise, the density decreases when $\partial v / \partial x$ is positive.

When $\bar{\rho}_0 > 1$, we know $\frac{\partial}{\partial x} v(x, 0) < 0$, and hence the density will initially increase (while remaining spatially uniform). Hence, $\bar{\rho}(t) \geq \bar{\rho}_0 > 1$, and thus $\frac{\partial}{\partial x} v(x, t) < 0$ for all t .

This shows that solutions will contract and blow up if the initial density $\bar{\rho}$ is sufficiently large; specifically, if $\bar{\rho}_0 > 1$. On the other hand, solutions will spread indefinitely if $\bar{\rho}_0 < 1$. At the critical density $\bar{\rho}_0 = 1$, we have an unstable steady state where social attraction precisely cancels external attraction.

Figure 8.1 shows numerical simulations that agree with these predictions.

While this example may seem somewhat contrived and perhaps physically implausible, it is significant in that it demonstrates the possibility of preventing blow-up via the addition of an external force. Next, we consider other ways of achieving the same result.

8.2 General Repulsive Potentials

More generally, we wish to determine sufficient conditions for preventing blow-up when F_s is a purely attractive social force and Q is an arbitrary attractive external potential. As in Chapter 5, we consider F_s with a jump discontinuity at the origin; i.e., where $\beta = \lim_{\varepsilon \downarrow 0} F_s(\varepsilon) < 0$. Moreover, it is

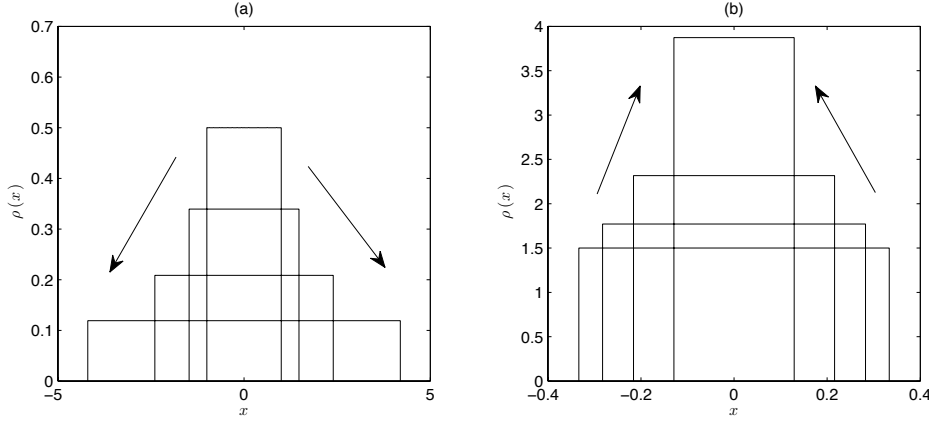


Figure 8.1: A simple system, in which $F_s = -\text{sgn}(r)$ and $Q(x) = -x^2$, illustrates that the asymptotic behavior of attractive swarms in repulsive potentials is dependent on initial conditions. For initial densities $\bar{\rho}_0 < 1$, solutions spread indefinitely, as shown in (a). For initial densities $\bar{\rho}_0 > 1$, solutions blow up, as shown in (b).

both mathematically convenient and physically reasonable to assume that the magnitude of the social force decays monotonically as the distance of separation increases. Then, we can express F_s as

$$F_s(r) = -|\beta|\text{sgn}(r) + g(r), \quad (8.6)$$

where g is continuously differentiable at the origin, and g' is everywhere non-negative.

Under our assumptions,

$$\begin{aligned} \frac{\partial}{\partial x} v(x, t) &= \int_{-\infty}^{\infty} \rho(z, t) F'_s(x - z) dz - Q''(x) \\ &= \int_{-\infty}^{\infty} \rho(z, t) [-2|\beta|\delta(x - z) + g'(x - z)] dz - Q''(x) \\ &= -2|\beta|\rho(x, t) + \int_{-\infty}^{\infty} \rho(z, t) g'(x - z) dz - Q''(x) \\ &\geq -2|\beta|\rho(x, t) - Q''(x). \end{aligned} \quad (8.7)$$

In neglecting the integral term, we have made use of our assumptions that ρ and g' are non-negative. Then, if we define

$$P(t) = \max_{z \in \mathbb{R}} \rho(z, t) \quad (8.8)$$

and

$$\zeta = \max_{x \in \mathbb{R}} Q''(x), \quad (8.9)$$

we have the following bound on $\partial v / \partial x$:

$$\frac{\partial}{\partial x} v(x, t) \geq -2|\beta|P(t) - \zeta. \quad (8.10)$$

Claim: If the maximum density $P(0)$ of the initial condition satisfies

$$P(0) < \frac{-\zeta}{2|\beta|}, \quad (8.11)$$

then the solution $\rho(x, t)$ cannot blow up.

Proof: If the above condition holds, then we can find $\varepsilon > 0$ such that

$$-2|\beta|P(0) - \zeta > \varepsilon > 0. \quad (8.12)$$

Applying (8.10) at $t = 0$, v_x is initially bounded by

$$v_x(x, 0) \geq -2|\beta|P(0) - \zeta > \varepsilon > 0. \quad (8.13)$$

By continuity, we can find some $T > 0$ such that $v_x(x, t) > \varepsilon$ for all $t \in [0, T]$ and all x in the support of $\rho(x, t)$. We choose T to be as large as possible and suppose, for the sake of contradiction, that T is finite. Then, at time T , $v_x(x, T) = \varepsilon$.

However, along characteristic curves $x(t)$ where $dx/dt = v$, the total derivative of the density is given by

$$\frac{d}{dt} \rho(x(t), t) = \rho_t + v \rho_x = -v_x \rho. \quad (8.14)$$

For $0 < t < T$, we know $v_x > \varepsilon > 0$. Since the characteristics are given by $dx/dt = v$, this means that the characteristic curves are initially rarefying, and therefore no shocks can form between $t = 0$ and $t = T$. Thus, the density varies continuously along characteristics.

Since the density is non-negative everywhere and $v_x > 0$,

$$\frac{d}{dt} \rho(x(t), t) < 0. \quad (0 < t < T) \quad (8.15)$$

Hence, the density strictly decreases along characteristics for $0 < t < T$. This implies that the maximum density is also strictly decreasing (i.e., $P(T) < P(0)$). Using (8.10) at $t = T$,

$$\begin{aligned} v_x(x, T) &\geq -2|\beta|P(T) - \zeta \\ &> -2|\beta|P(0) - \zeta \\ &> \varepsilon. \end{aligned} \quad (8.16)$$

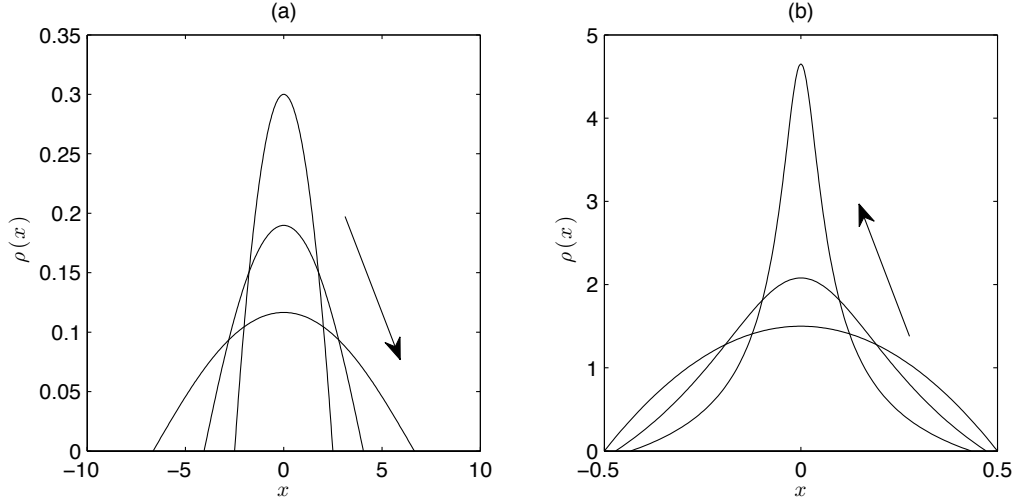


Figure 8.2: In this system, $F_s(r) = -\text{sgn}(r)e^{-|r|}$ and $Q(x) = -x^2$. In (a), the maximum initial density is small enough to avoid blow-up. In (b), however, we see that higher initial densities can still lead to blow-up.

However, this contradicts $v_x(x, T) = \varepsilon$. We conclude that $v_x(x, t) > \varepsilon > 0$ for all $t > 0$. From (8.14), we see that the density is strictly decreasing along characteristics for all time. This shows that the solution can never blow up, concluding our proof.

Numerical tests were run using

$$Q(x) = -\frac{1}{2}x^2 \quad \text{and} \quad F_s(r) = -\text{sgn}(r)e^{-|r|}, \quad (8.17)$$

so that

$$\zeta = \max Q''(x) = -1 \quad \text{and} \quad \beta = \lim_{r \downarrow 0} F_s(r) = -1. \quad (8.18)$$

In this case, condition (8.11) implies that thinning is guaranteed when

$$\max \rho(x, 0) < 1/2. \quad (8.19)$$

Figure 8.2 shows simulation results that agree with this prediction.

8.3 Physically Relevant Scenarios

The above conditions imply that for an external potential to prevent blow-up, Q'' must be sufficiently negative over its entire domain. However, this

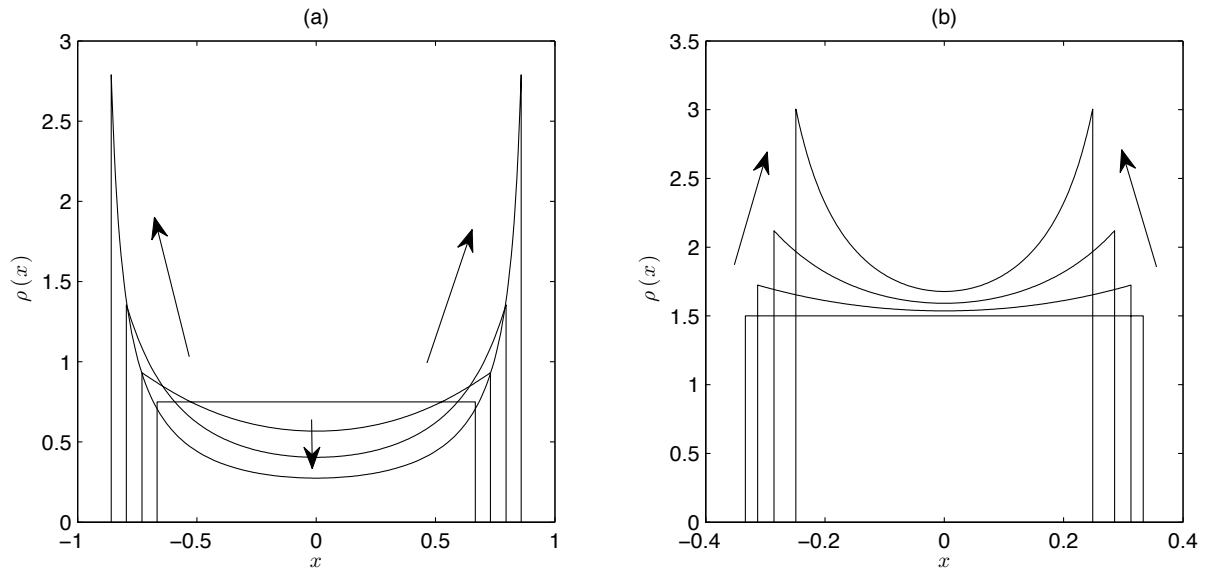


Figure 8.3: In this system, the social force is $F_s(r) = -\text{sgn}(r)e^{-|r|}$ and the external potential is an inverted gaussian, given by $Q(x) = -e^{-x^2}$. Since the external potential becomes negligible as $|x| \rightarrow \pm\infty$, we cannot guarantee the prevention of blow-up. In (a), the initial density is small, leading to a thinning region between two growing peaks. In (b), the initial density is large, leading to collapse into a single δ -function.

would mean that the magnitude of the external repulsive force grows arbitrarily large as we move away from the origin.

To consider physically plausible systems, we should require $|F_c(x)| \rightarrow 0$ as $|x| \rightarrow \pm\infty$. Hence, $Q''(x) \rightarrow 0$ as $|x| \rightarrow \pm\infty$, and therefore we can never use condition (8.11) to guarantee the prevention of blow-up.

In numerical tests using physically plausible potentials, the density was always observed to blow-up; if the initial density is high, the swarm collapses to a single point (as it would without any external potential), whereas low initial density causes blow-up to occur at two separate peaks separated by a thinning section. An example of this behavior is shown in Figure 8.3.

Chapter 9

Repulsive Swarms in Attractive Potentials

Next, we study swarms with pure social repulsion placed inside an attractive potential. Our main goal here is to determine when it is possible for the attractive potential to turn spreading into steady states. For simplicity, we assume in this section that the social force is given by

$$F_s(r) = \operatorname{sgn}(r) e^{-|r|}. \quad (9.1)$$

We expect that an analysis similar to the following should be possible for other choices of F_s , but the results are particularly elegant for this social force.

9.1 Necessary Conditions for Steady-State Solutions

The following analysis provides us with necessary conditions for the existence of steady-state solutions. Suppose we have a steady-state solution $\rho(x)$ with compact support on the interval $[-b, b]$. Then $\rho_t = 0$ and the governing equations imply $(\rho v)_x = 0$. Integrating with respect to x , we have $\rho v = 0$. Note that the constant of integration must be zero because $\rho = 0$ for $x \notin [-b, b]$. Now, wherever $\rho \neq 0$ (i.e., inside $[-b, b]$), we must have $v = 0$. Hence,

$$\int_{-\infty}^{\infty} \rho(z) F_s(x-z) dz = Q'(x) \quad (-b \leq x \leq b). \quad (9.2)$$

For our particular choice of F_s , we have

$$\int_{-\infty}^{\infty} \rho(z) \operatorname{sgn}(x-z) e^{-|x-z|} dz = Q'(x) \quad (-b \leq x \leq b). \quad (9.3)$$

Following the argument used by Bernoff and Topaz in [1], we can apply the linear operator $\mathcal{L} = \partial_{xx} - 1$ to both sides to annihilate the integral expression, obtaining

$$2\rho_x = Q'''(x) - Q'(x) \quad (-b \leq x \leq b). \quad (9.4)$$

After integrating both sides with respect to x , we have

$$\rho(x) = \begin{cases} \frac{1}{2}(Q''(x) - Q(x) + \lambda), & |x| \leq b, \\ 0, & |x| > b. \end{cases} \quad (9.5)$$

To compute the constant of integration λ , we substitute this solution (9.5) into the integral equation (9.3), obtaining

$$\begin{aligned} Q'(x) &= Q'(x) + e^{-x} \left[\frac{e^b}{2} (Q(-b) - Q'(-b) - \lambda) \right] \\ &\quad - e^x \left[\frac{e^{-b}}{2} (Q(b) + Q'(b) - \lambda) \right]. \end{aligned} \quad (9.6)$$

For this to hold, we require

$$Q(b) + Q'(b) - \lambda = 0 \quad \text{and} \quad Q(-b) - Q'(-b) = 0, \quad (9.7)$$

since e^x and e^{-x} are linearly independent. However, since Q is assumed to be symmetric (and therefore Q' is antisymmetric), these two conditions are equivalent, and therefore the integral equation (9.3) is solved provided

$$\lambda = Q(b) + Q'(b). \quad (9.8)$$

Hence,

$$\rho(x) = \begin{cases} \frac{1}{2}(Q''(x) - Q(x) + Q(b) + Q'(b)), & |x| \leq b, \\ 0, & |x| > b. \end{cases} \quad (9.9)$$

If we specify the mass M of the system, then we obtain the following, via integration by parts and a good deal of algebraic manipulation:

$$M = \int_{-\infty}^{\infty} \rho(z) dz \quad (9.10)$$

$$= \int_{-b}^b \frac{Q''(z) - Q(z) + Q(b) + Q'(b)}{2} dz \quad (9.11)$$

$$= \int_0^b (z+1) (Q''(z) + Q'(z)) dz \quad (9.12)$$

Now we define

$$\mu_Q(x) = \int_0^x (z+1)(Q''(z) + Q'(z)) dz, \quad (9.13)$$

so that a necessary condition for the existence of a steady-state solution is simply

$$\mu_Q(b) = M. \quad (9.14)$$

This implies that solutions of mass M on the interval $[-b, b]$ can only exist when (b, M) lies on the curve $M = \mu_Q(b)$.

9.2 Finite-Capacity and Infinite-Capacity Potentials

The function μ_Q determines which combinations of swarm width and swarm mass are allowable in steady-state solutions. Moreover, we conjecture that μ_Q can be used to identify which potentials can accommodate steady-state solutions of arbitrarily large mass.

We say a potential has *infinite capacity* if, for all $M > 0$, we can find a non-negative steady-state solution with mass M . We say a potential has *finite capacity* if there exists some $M^* > 0$ such that no non-negative steady-state solution exists with mass $M > M^*$.

We conjecture that if μ_Q grows without bound, then Q has infinite capacity. On the other hand, if μ_Q has an upper bound, then we conjecture that Q has finite capacity given by $\sup \mu_Q(x)$.

9.3 Example I: An Infinite-Capacity Potential

Consider the external attractive potential

$$Q(x) = x^2. \quad (9.15)$$

From (9.13),

$$\mu_Q(x) = \int_0^x (z+1)(2+2z) dz \quad (9.16)$$

$$= \frac{2}{3} ((x+1)^3 - 1). \quad (9.17)$$

Note that μ_Q increases monotonically and without bound, which means it fits our conjectured criteria for potentials with infinite capacity.

For a steady-state solution of mass M to exist on the interval $[-b, b]$, we require $\mu_Q(b) = M$. That is,

$$\frac{2}{3}((b+1)^3 - 1) = M. \quad (9.18)$$

For each positive value of M , we see that there is exactly one positive solution b :

$$b = \left(1 + \frac{3M}{2}\right)^{1/3} - 1. \quad (9.19)$$

Now, from (9.9), we have

$$\rho(x) = \begin{cases} -\frac{1}{2}x^2 + \frac{1}{2}b^2 + 1 + b, & |x| \leq b, \\ 0, & \text{otherwise.} \end{cases} \quad (9.20)$$

Note that, for $|x| \leq b$, this solution is a downward-facing parabola; this means that its minimum nonzero value occurs at $x = \pm b$, and we can easily verify that this value is positive:

$$\min \rho(x) = \rho(b) = 1 + b = \left(1 + \frac{3M}{2}\right)^{1/3} > 1. \quad (9.21)$$

This demonstrates that we can find a non-negative steady-state solution with finite width for any mass $M > 0$. Thus, $Q(x) = x^2$ is indeed an infinite-capacity potential.

Figure 9.1 shows a numerical solution approaching the steady-state solution associated with $b = 1$ and $M = \mu_Q(1) = 14/3$. Figure 9.2 shows the steady-state solutions predicted for $M = 1, 2, 3, 4$.

9.4 Example II: A Finite-Capacity Potential

Now consider the external attractive potential

$$Q(x) = -e^{-x^2}. \quad (9.22)$$

From (9.13), we compute

$$\mu_Q(x) = -2 \int_0^x (z+1)(z-1)(2z+1)e^{-z^2} dz \quad (9.23)$$

$$= (x + 2x^2)e^{-x^2} + \frac{\sqrt{\pi}}{2} \operatorname{erf}(x). \quad (9.24)$$

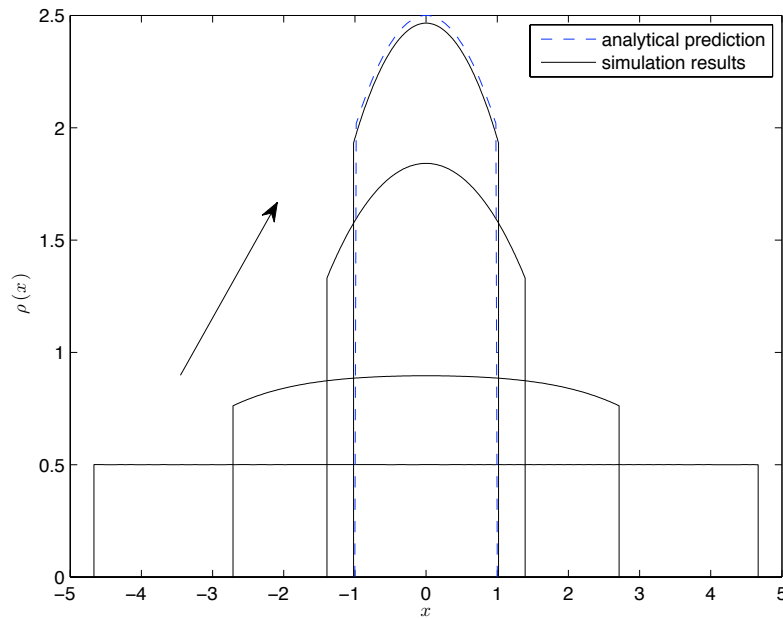


Figure 9.1: Simulation results approach the predicted equilibrium solution for a repulsive social force $F_s(r) = \text{sgn}(r)e^{-|r|}$ inside an attractive external potential $Q(x) = x^2$. The initial condition has mass $M = 14/3$, and the exact equilibrium solution was predicted by setting $b = \mu_Q^{-1}(M) = 1$ in (9.20).

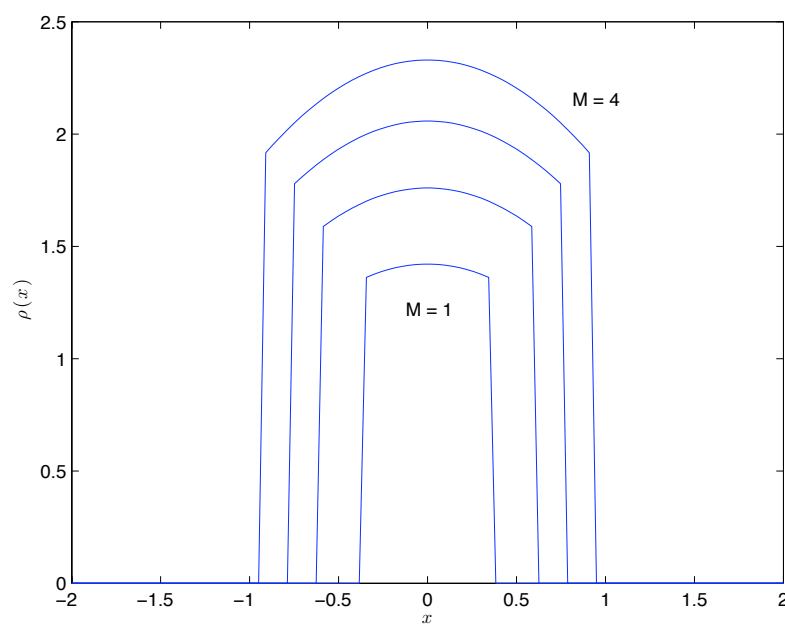


Figure 9.2: A family of equilibrium solutions for $F_s(r) = \text{sgn}(r)e^{-|r|}$ inside the attractive potential $Q(x) = x^2$. These solutions were computed by setting $b = \mu_Q^{-1}(M)$ in (9.20).

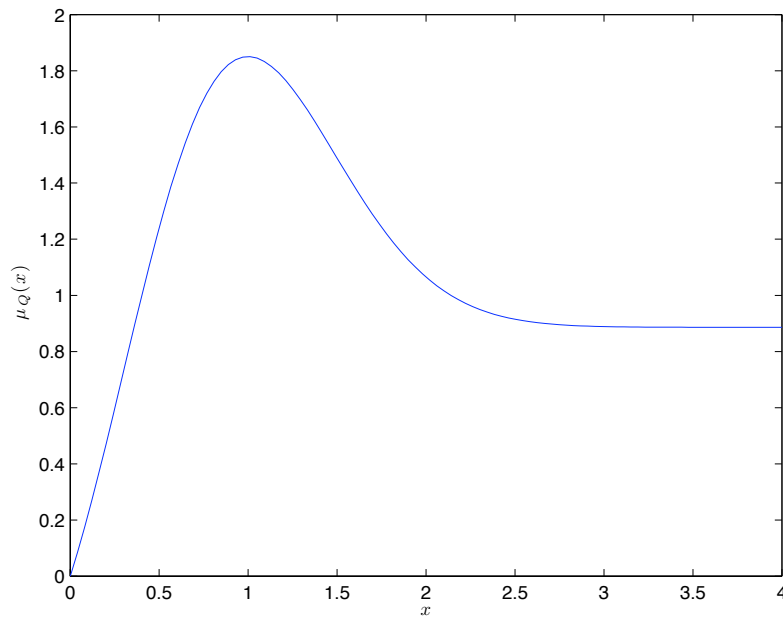


Figure 9.3: A plot of $\mu_Q(x) = (x + 2x^2)e^{-x^2} + \frac{\sqrt{\pi}}{2} \operatorname{erf}(x)$, which is associated with the attractive inverted gaussian potential $Q(x) = -e^{-x^2}$ and social force $F_s = \operatorname{sgn}(r)e^{-|r|}$. Since μ_Q never exceeds $M^* \approx 1.85$, we conclude that Q is a finite-capacity potential.

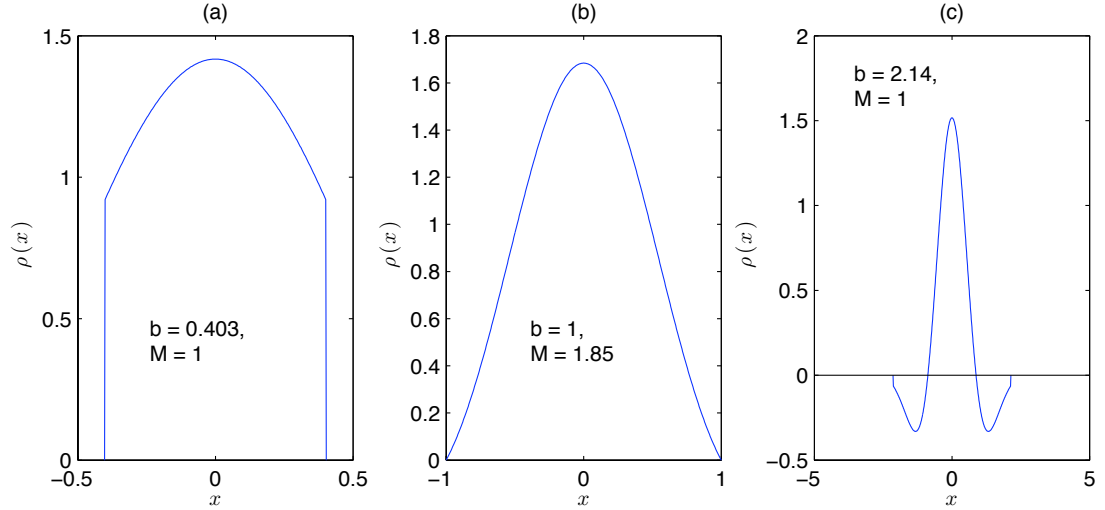


Figure 9.4: Steady-state solutions associated with $Q(x) = -e^{-x^2}$ and $F_s = \text{sgn}(r)e^{-|r|}$. Panels (a) and (c) show two distinct steady-state solutions of mass $M = 1$. Since the solution in (c) achieves negative values, we can reasonably expect that initial conditions of mass $M = 1$ will approach the solution shown in (a) rather than the solution shown in (c). Panel (b) shows a solution of intermediate width and maximum possible mass $M = M^* \approx 1.85$. These solutions were computed by setting $b = 0.403$, $b = 1$, and $b = 2.14$, respectively, in (9.28).

Figure 9.3 shows a plot of μ_Q . We can see that the maximum value of μ_Q occurs at $x = 1$, since

$$\mu'_Q(x) = (x+1)(Q''(x) + Q'(x)) \quad (9.25)$$

$$= -2(x+1)(x-1)(2x+1)e^{-x^2}. \quad (9.26)$$

In particular,

$$\max \mu_Q(x) = \mu_Q(1) = 3e^{-1} + \frac{\sqrt{\pi} \text{erf}(1)}{2} \approx 1.85. \quad (9.27)$$

Since $\mu_Q(b) = M$ is a necessary condition for the existence of a steady-state solution of mass M on the interval $[-b, b]$, there can be no steady-state solutions with mass $M > \max \mu_Q$. In other words, this potential has finite capacity $M^* \approx 1.85$.

Now, for any swarm width $b > 0$, we can compute the steady-state solution on the interval $[-b, b]$ with mass $M = \mu_Q(b)$ using (9.9):

$$\rho(x) = \begin{cases} \left(\frac{3}{2} - 2x^2\right) e^{-x^2} + \left(b - \frac{1}{2}\right) e^{-b^2}, & |x| \leq b, \\ 0, & |x| > b. \end{cases} \quad (9.28)$$

As Figure 9.4 illustrates, these solutions may achieve negative values. Therefore, we wish to determine conditions that guarantee the non-negativity of $\rho(x)$. Using (9.9), we compute the slope of the density on the interval $[-b, b]$:

$$\rho'(x) = \frac{1}{2} (Q'''(x) - Q'(x)) \quad (9.29)$$

$$= x(4x^2 - 7)e^{-x^2}. \quad (9.30)$$

From this, we see that if the swarm width $b < \sqrt{7}/2$, then the minimum nonzero value of $\rho(x)$ must occur at $x = \pm b$, the endpoints of the swarm. Hence, for the case $b < \sqrt{7}/2$, we need only check the non-negativity of $\rho(b)$. Referring once again to (9.9), the endpoint density is given by

$$\rho(b) = \frac{1}{2} (Q''(b) + Q'(b)) \quad (9.31)$$

$$= -(2b + 1)(b - 1)e^{-b^2}. \quad (9.32)$$

This shows that the endpoint density is positive when $b < 1$ and negative when $b > 1$. Since $1 < \sqrt{7}/2$, we know that $b < 1$ guarantees that the minimum nonzero value of $\rho(x)$ occurs at the endpoints. Hence, $\rho(x)$ stays non-negative if and only if $b < 1$. This corresponds exactly to the interval on which μ_Q is increasing. Hence, if we restrict the domain of μ_Q to $0 < x < 1$, this makes it one-to-one, and we can solve uniquely for the equilibrium swarm width $b = \mu_Q^{-1}(M)$, provided $M < M^*$.

As an aside, we note briefly that there is a simple relationship between μ'_Q and the endpoint density $\rho(b)$. From (9.25) and (9.31),

$$2(b + 1)\rho(b) = \mu'_Q(b). \quad (9.33)$$

Considering only $b > 0$, we see that $\mu'_Q(b) < 0$ implies that a steady-state swarm of width b has negative density at its endpoints. On the other hand, $\mu'_Q(b) > 0$ implies that a steady-state swarm of width b has positive density at its endpoints. In general, however, $\mu'_Q(b) < 0$ is not sufficient to guarantee non-negativity of $\rho(x)$ on the whole interval $[-b, b]$. To do so

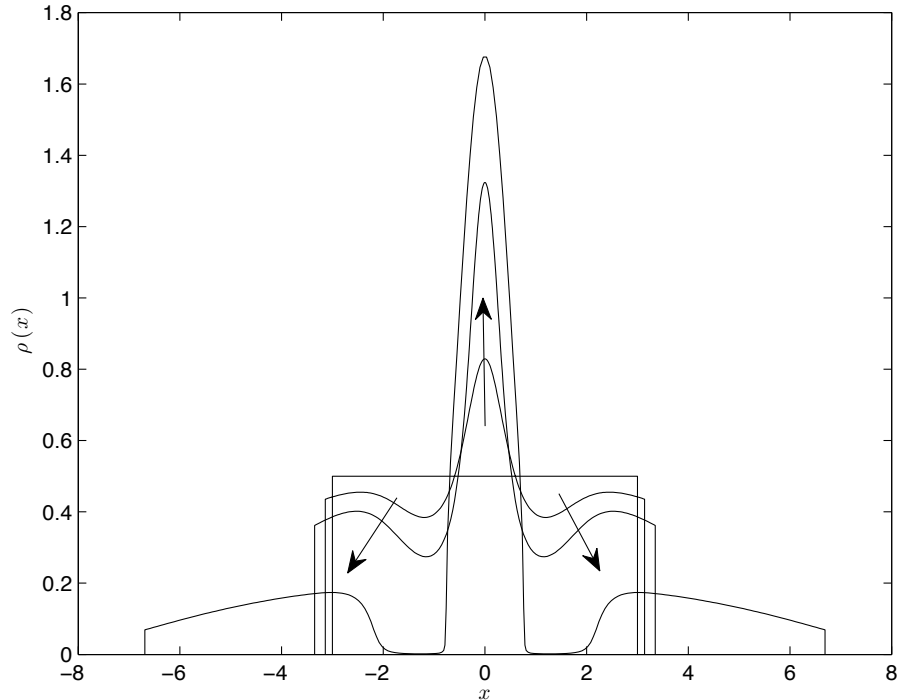


Figure 9.5: For $F_s = \text{sgn}(r)e^{-|r|}$ and $Q(x) = -e^{-x^2}$, an initial condition with mass $M > M^*$ spreads indefinitely. The stable peak that appears in the center of the solution is approximately equal to the critical steady-state solution of mass $M^* \approx 1.85$, shown in Figure 9.4.b.

requires additional checks on the location of local maxima and minima of $\rho(x)$, which we performed in (9.30).

Figure 9.5 shows the result of a simulation in which $M > M^*$. Since the mass of the swarm exceeds the potential's capacity, the solution spreads indefinitely. Curiously, however, a stable peak persists at the center of this spreading solution. This stable central peak appears very similar to the critical steady-state solution of mass $M^* \approx 1.85$. Moreover, a thinning strip of mass connects the central peak to the exterior spreading portions. As shown in Figure 9.6, the spreading portions closely match half-parabolas, which we conjecture may be related to spreading Barenblatt solutions of the porous-medium equation.

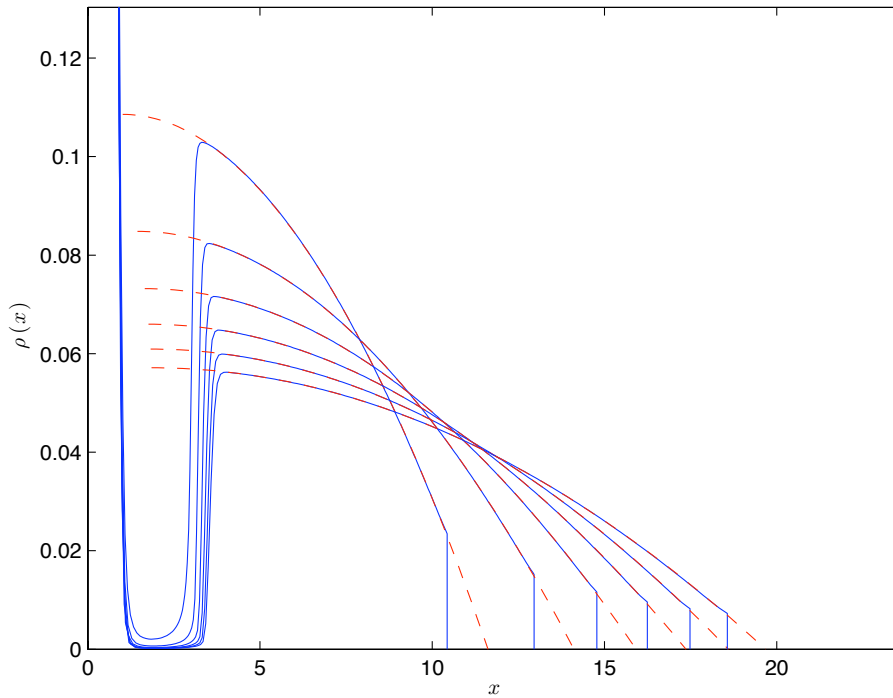


Figure 9.6: The spreading portions of the solution of Figure 9.5 closely match half-parabolas. Since the potential Q becomes negligible for large $|x|$, we conjecture that the spreading portions are related to Barenblatt's spreading solutions to the porous-medium equation, as we found to be the case in the absence of any external potential (Section 3.1).

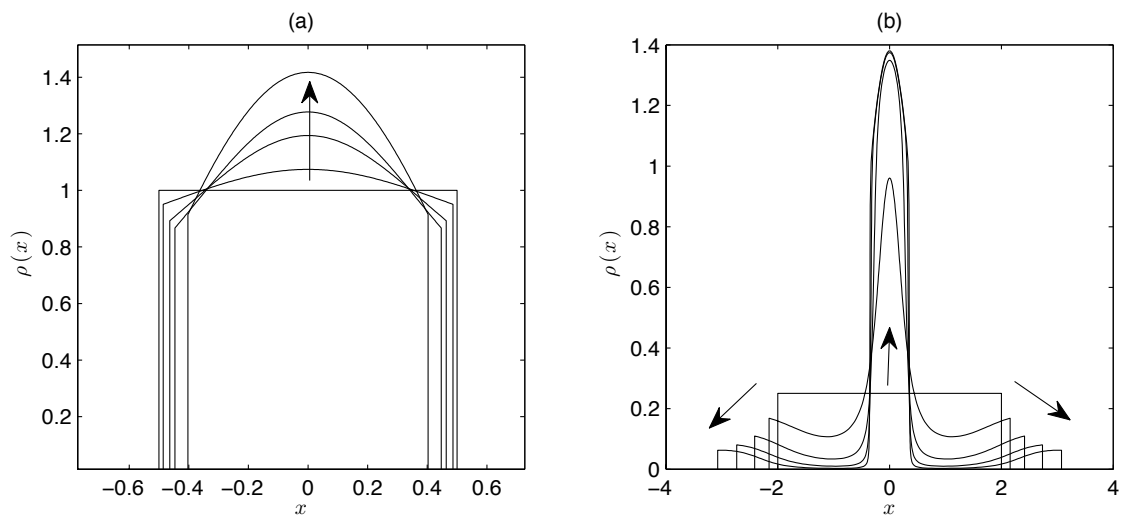


Figure 9.7: For $F_s = \text{sgn}(r)e^{-|r|}$ and $Q(x) = -e^{-x^2}$, initial conditions of mass $M = 1 < M^*$ may behave differently depending on their initial width. In (a), a narrow initial condition approaches the steady-state solution shown in Figure 9.4.a. Panel (b) shows that some mass can escape the attractive potential and spread indefinitely if the initial condition is sufficiently wide.

On the other hand, Figure 9.7 shows the results of two different simulations in which $M < M^*$. Although we have predicted the existence of a steady-state solution in this case, it is not globally attracting, and certain initial conditions fail to approach it. A narrow initial condition approaches our predicted steady-state solution; however, a wide initial condition leads to spreading (much like the the case where $M > M^*$). Presumably, this spreading is due to the weakness of the external attractive force far from the origin.

9.5 Example III: Looking for an Unusual Potential

In Example I, we saw an infinite-capacity potential for which μ_Q grows without bound. In Example II, we saw a finite-capacity potential for which μ_Q is sometimes decreasing. It is therefore interesting to consider what might happen if μ_Q grows without bound but is sometimes decreasing. Specifically, would such a potential have finite or infinite capacity? In what follows, we construct such a potential and determine, via numerical tests, that it appears to have infinite capacity; at the same time, the results suggest that there exist some positive reals b such that no non-negative steady-state solutions exist on the interval $[-b, b]$.

9.5.1 Constructing a Potential Q from μ_Q

Instead of specifying a potential Q (or, equivalently, a social force F_c) and then computing μ_Q , it is possible to specify μ_Q and then find the corresponding potential. For example, suppose we specify

$$\mu_Q(x) = h(x), \tag{9.34}$$

where $h(x) \geq 0$ for $x > 0$, and $h(0) = 0$. Then for $x > 0$,

$$h(x) = \int_0^x (z+1)(Q''(z) + Q'(z)) dx. \tag{9.35}$$

Next, we differentiate both sides and obtain

$$h'(x) = (x+1)(Q''(x) + Q'(x)). \tag{9.36}$$

Using an integrating factor,

$$\frac{h'(x)e^x}{x+1} = e^x Q''(x) + e^x Q'(x) = \frac{d}{dx} [e^x Q'(x)]. \tag{9.37}$$

Taking a definite integral on both sides,

$$\int_0^x \frac{h'(z)e^z}{z+1} dz = e^x Q'(x) - e^0 Q'(0). \quad (9.38)$$

Now, we solve for $Q'(x)$ when $x > 0$:

$$Q'(x) = e^{-x} \left[\int_0^x \frac{h'(z)e^z}{z+1} dz + Q'(0) \right]. \quad (9.39)$$

If we assume Q is differentiable at the origin, then $Q'(0) = 0$ by symmetry, and when $x > 0$,

$$Q'(x) = e^{-x} \int_0^x \frac{h'(z)e^z}{z+1} dz. \quad (9.40)$$

Knowing $Q'(x)$ for $x > 0$, we can construct $F_c(x)$ for all x using symmetry:

$$F_c(x) = -Q'(x) \quad (9.41)$$

$$= -\text{sgn}(x)Q'(|x|) \quad (9.42)$$

$$= -\text{sgn}(x)e^{-|x|} \int_0^{|x|} \frac{h'(z)e^z}{z+1} dz. \quad (9.43)$$

This construction allows us to find potentials Q for which the associated functions μ_Q exhibit a particular desired behavior. We will now apply this construction to obtain a potential for which μ_Q decreases over a finite range, but ultimately increases without bound.

9.5.2 Applying the Construction

Consider the function

$$h(x) = \frac{x^3}{3} - \frac{3x^2}{2} + 2x, \quad (9.44)$$

which decreases over the interval $1 < x < 2$ and increases without bound as $x \rightarrow \infty$. If we specify $\mu_Q = h(x)$, then (9.43) yields

$$F_c(x) = -\text{sgn}(x)e^{-|x|} \int_0^{|x|} \frac{e^z h'(z)}{z+1} dz \quad (9.45)$$

$$= -\text{sgn}(x)e^{-|x|} \int_0^{|x|} \frac{e^z (z^2 - 3z + 2)}{z+1} dz. \quad (9.46)$$

For the purposes of simulation, we can evaluate F_c numerically over a finite interval. Since $h(x)$ is not bounded from above, we conjecture that this

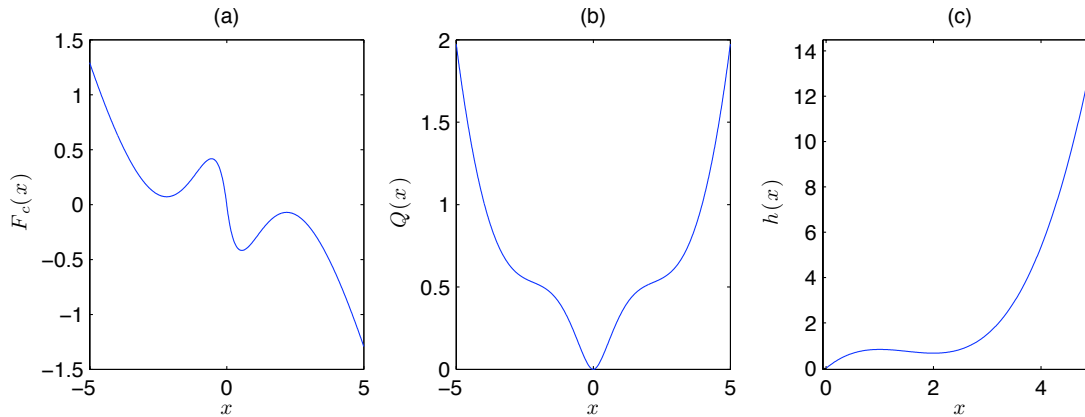


Figure 9.8: (a) The external force F_s obtained by setting $\mu_Q(x) = \frac{x^3}{3} - \frac{3x^2}{2} + 2x$. (b) The associated external potential Q . (c) The function $h(x) = \mu_Q(x) = \frac{x^3}{3} - \frac{3x^2}{2} + 2x$.

potential has infinite capacity. Figure 9.8.a shows the shape of F_c ; Figure 9.8.b shows the shape of the associated potential Q ; and Figure 9.8.c shows the function $h(x) = \mu_Q(x)$.

Note that the only local maximum of $h(x)$ occurs at $(1, 5/6)$, and the only local minimum occurs at $(2, 2/3)$. For $0 < x < 1$, $h(x)$ is single-valued, but for $1 < x < 5/2$, the function repeats previously-achieved values. When $x > 5/2$, $h(x)$ once again becomes single-valued. Hence, when $M < 2/3$ or $M > 5/6$, we can find a unique solution to $M = \mu_Q(b) = h(b)$. When $2/3 < M < 5/6$, however, there are three such solutions. If we specify a mass M within this range, we conjecture that the equilibrium solution corresponds to smallest positive value of b solving $M = h(b)$.

The results of a simulation where $M < 5/6$ are shown in Figure 9.9.a. Qualitatively, the equilibrium solution approached in this simulation is not drastically different from other equilibria we've previously seen. The sharp peak is new, however; it arises from the fact that Q'' is not smooth at the origin.

Figure 9.9.b shows the results of a simulation where $M > 5/6$. In this case, we observe a steady-state solution whose support is not a single interval, but rather the union of three disjoint intervals. Note that the analysis we used above to find steady-state solutions does not allow for the possibility of the density reaching zero on the interval $[-b, b]$, and so in this case we should not expect our analytical results to accurately predict the

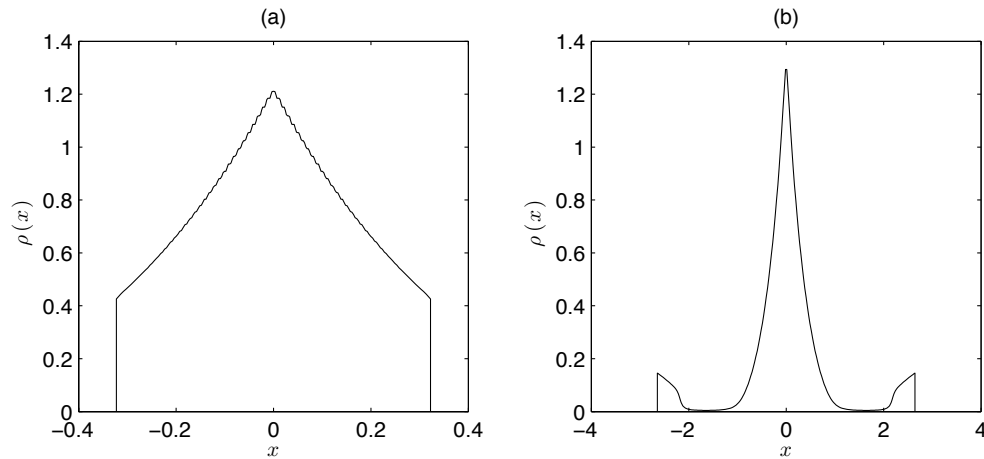


Figure 9.9: Steady states for the external force (9.46), obtained via numerical simulation. An initial condition of mass $M = 1/2$ approached the solution shown in (a), and an initial condition of mass $M = 1$ approached the solution shown in (b). Interestingly, the density of the latter steady state appears to reach zero, which may render (9.9), our formula for exact steady-state solutions, inapplicable to this particular case.

observed steady-state solution.

This potential is difficult to analyze due to the complexity of our formula for F_c , but its unusual steady-state behavior warrants further study.

Chapter 10

Conclusions and Future Work

These results provide us with an understanding of the different types of asymptotic behavior of this system, especially in the case where we use the Morse interaction force.

For a general interaction force, we predicted the asymptotic behavior of the system for long-wave and short-wave initial conditions. Short waves behave for at least a short time according to Burgers' equation, and, similarly, long waves behave for at least a short time according to the porous-medium equation. Combining these results, and using the fact that the effect of short-wave instability naturally dominates long-wave stability, we found conditions on the social interaction force F_s leading to the following three asymptotic behaviors:

- Blow-up (whenever short waves contract)
- Spreading (when both short waves and long waves expand)
- Steady-state (when short waves expand and long waves contract)

Subsequently, we arrived at more quantitative predictions for each category of behavior. In the blow-up regime, we found an upper bound for the time to blow-up, which applies for arbitrary interaction forces. In the spreading regime, we found a traveling-wave solution that approximates the edge behavior for spreading solutions in the case where F_s is a Morse interaction force. In the steady-state regime, we used previous results to find equilibrium solutions, once again assuming a Morse interaction force.

Finally, we studied the effect of incorporating external forces via several specific examples. We discovered that it is possible to qualitatively

change the asymptotic behavior of the system (for example, from spreading to steady-state, or from blow-up to spreading) simply by adding an external potential.

Some natural extensions to this work might include translating these results into higher dimensions or predicting the qualitative behavior of the system for fully arbitrary combinations of social forces and external potentials.

Appendix A

Numerical Methods

A.1 Discrete Swarming Model

The continuous swarming model studied above can be thought of as the limit of a discrete swarming model as the number of individuals goes to infinity. For a finite swarm of size N in one spatial dimension, we let $x_i(t)$ denote the position of the i th individual at time t and let m_i denote the mass of the i th individual. Then, the motion of the swarm is governed by the following set of N ordinary differential equations:

$$\frac{dx_i}{dt} = \sum_{j \neq i} m_j F_s(x_i - x_j). \quad (\text{A.1})$$

A.2 The Numerical Algorithm

To simulate the original continuous PDE, we translate the continuous IC into a discrete IC having approximately the same mass distribution, and we simply solve the above system of ODEs numerically. In post-processing, we find the cumulative mass function

$$\psi(x, t) = \sum_{\{i: x_i(t) < x\}} m_i, \quad (\text{A.2})$$

which we can numerically differentiate via interpolation to find the corresponding density. The following arguments support the validity of this method, assuming we don't deal with pathological cases.

A.3 Convergence

If we allow the number of individuals N to grow without bound and assign each individual a mass $m_i = M/N$, so that the total mass does not increase, the behavior of the swarm essentially approaches that of the continuous system. To see this, note that the cumulative mass function $\psi(x, t) = \int_{-\infty}^x \rho(z, t) dz$ is well-defined in both the continuous case and the discrete case. (Note: In the discrete case, the density is essentially a superposition of point masses which can be modeled as δ -functions, and the above integral becomes a sum.) Hence, when we say that the discrete model converges to the continuous model, we mean that the discrete cumulative mass function $\psi_N(x, t)$ converges to the continuous cumulative mass function $\psi(x, t)$, provided that the sequence of initial conditions $\psi_N(x, 0)$ converge to the continuous initial condition $\psi(x, 0)$.

If we define $\zeta_\mu(t)$ for $\mu \in (0, 1)$ such that

$$\psi(\zeta_\mu(t), t) = \int_{-\infty}^{\zeta_\mu(t)} \rho(z, t) dz = \mu M, \quad (\text{A.3})$$

we can show that $d\zeta_\mu/dt = v(\zeta_\mu(t), t)$ using Leibniz's rule. Hence, if we can find an expression for the motion of $\zeta_\mu(t)$ for a large number of values of μ , we obtain an approximation for the cumulative mass function $\psi(x, t)$ corresponding to a solution of the original continuous PDE.

The following is a proof of the above claim.

Differentiating both sides with respect to t using Leibniz's rule,

$$\rho(\zeta_\mu(t), t) \cdot \zeta'_\mu(t) + \int_{-\infty}^{\zeta_\mu(t)} \frac{\partial}{\partial t} \rho(z, t) dz = 0. \quad (\text{A.4})$$

If we assume ρ solves the continuous equation, we can substitute $\rho_t = -(v\rho)_x$, yielding

$$\rho(\zeta_\mu(t), t) \cdot \zeta'_\mu(t) - \int_{-\infty}^{\zeta_\mu(t)} \frac{\partial}{\partial z} (\rho(z, t) \cdot v(z, t)) dz = 0. \quad (\text{A.5})$$

Using the fundamental theorem of calculus and assuming ρ approaches zero as $x \rightarrow \pm\infty$, this becomes

$$\rho(\zeta_\mu(t), t) \cdot \zeta'_\mu(t) = \rho(\zeta_\mu(t), t) \cdot v(\zeta_\mu(t), t). \quad (\text{A.6})$$

Then, assuming the support of the swarm is a simply connected interval, $\rho(\zeta_\mu(t), t) > 0$, and thus $\zeta'_\mu(t) = v(\zeta_\mu(t), t)$. That is, at time t , ζ_μ moves with speed $v(\zeta_\mu(t), t)$.

Furthermore, we can approximate the velocity at each point in a solution to the continuous PDE by using a midpoint rule to evaluate the relevant integral expression, and we ultimately find that the velocity under this approximation has the same form as the discrete velocity.

To be precise, we wish to compute the error in using the discrete approximation

$$v(x_i, t) \approx F_c(x_i) + \sum_{j \neq i} m_j F_s(x_i - x_j). \quad (\text{A.7})$$

In the continuous case, the expression for the velocity is

$$v(x, t) = \int_{-\infty}^{\infty} \rho(\tilde{x}, t) F_s(x - \tilde{x}) d\tilde{x}, \quad (\text{A.8})$$

If we define $P_t(x) = \int_{-\infty}^x \rho(\tilde{x}, t) d\tilde{x}$, then $\rho(\tilde{x}, t) = P_t'(\tilde{x})$. Therefore, v simplifies to

$$v(x, t) = \int_0^M F_s(x - P_t^{-1}(p)) dp, \quad (\text{A.9})$$

where $M = \int_{-\infty}^{\infty} \rho(x, 0) dx$ is the total mass of the system.

Next, we will apply the midpoint rule to approximate this integral. Define

$$b_j = \begin{cases} 0 & j = 0, \\ \sum_{k=1}^j m_k & j > 0, \end{cases} \quad (\text{A.10})$$

and

$$p_j = \frac{m_j}{2} + b_{j-1} \quad (j = 1, 2, 3, \dots). \quad (\text{A.11})$$

Then, if we define intervals $\Omega_j = (b_{j-1}, b_j)$, the points p_j represent the midpoints of these intervals.

We can rewrite the above integral as

$$\int_0^M F_s(x - P_t^{-1}(p)) dp = \sum_{j=1}^N \int_{\Omega_j} F_s(x - P_t^{-1}(p)) dp \quad (\text{A.12})$$

For convenience, let $f(p) = F_s(x - P_t^{-1}(p))$. Then, expanding f about p_j yields

$$f(p) = f(p_j) + (p - p_j)f'(p_j) + \frac{1}{2}(p - p_j)^2 f''(\xi_j) \quad (\text{A.13})$$

for some ξ_j satisfying $|\xi_j - p_j| < |p - p_j|$.

Then, considering the j th term on the right-hand side of equation (A.12),

$$\begin{aligned}\int_{\Omega_j} f(p) dp &= \int_{\Omega_j} \left(f(p_j) + (p - p_j)f'(p_j) + \frac{1}{2}(p - p_j)^2 f''(\xi_j) \right) dp \\ &= \int_{-m_j/2}^{m_j/2} \left(f(p_j) + zf'(p_j) + \frac{1}{2}z^2 f''(\xi_j) \right) dz \\ &= m_j f(p_j) + \frac{m_j^3}{24} f''(\xi_j) \\ &= m_j F_s(x - P_t^{-1}(p_j)) + \frac{m_j^3}{24} f''(\xi_j).\end{aligned}\tag{A.14}$$

If we assume the ratio of the maximum of the m_i 's to the average of the m_i 's is bounded as the number of individuals increases, we see that this error is of the order $\mathcal{O}(N^{-2})$.

Next, we note that the interpolation used in finding the density has a maximum error that depends on how many points are used. Similarly, the derivative of the interpolating polynomial, used as an approximation for the density $\rho(x, t)$, has some related (and easy-to-compute) error.

Note that the error here being small depends on the spacing being approximately even. To guarantee that this is the case, we can periodically redistribute the mass of the system over uniformly-spaced set of points (i.e., "re-grid") whenever the spacing becomes too uneven.

Bibliography

- [1] A. Bernoff and C. Topaz. Equilibrium Configurations of Interacting Particles in One Dimension. Preprint, 2008.
- [2] A. Bertozzi and T. Laurent. Finite-Time Blow-Up of Solutions of an Aggregation Equation in \mathbb{R}^n . *Communications in Mathematical Physics*, 274.3:717–735, 2007.
- [3] M. Bodnar and J.J.L. Velazquez. Derivation of Macroscopic Equations for Individual Cell-Based Models: A Formal Approach. *Mathematical Methods in the Applied Science*, 28:1757–1779, 2005.
- [4] M. Bodnar and J.J.L. Velazquez. An Integro-Differential Equation Arising as a Limit of Individual Cell-Based Models. *Journal of Differential Equations*, 222:341–380, 2006.
- [5] Y. Chuang, M. D’Orsogna, D. Marthaler, A. Bertozzi, and L. Chayes. State Transitions and the Continuum Limit for a 2D Interacting, Self-Propelled Particle System. *Physica D: Nonlinear Phenomena*, 232.1:33–47, 2007.
- [6] M.R. D’Orsogna, Y.L. Chuang, A.L. Bertozzi, and L.S. Chayes. Self-Propelled Particles with Soft-Core Interactions: Patterns, Stability, and Collapse. *Physical Review Letters*, 96:104302, 2006.
- [7] R. Eftimie, G. de Vries, and M.A. Lewis. Complex Spatial Group Patterns Result from Different Animal Communication Mechanisms. *Proceedings of the National Academy of Sciences*, 104:6974–6979, 2007.
- [8] A. Mogilner and L. Edelstein-Keshet. A Non-Local Model for a Swarm. *Journal of Mathematical Biology*, 38:534–570, 1999.

- [9] A. Mogilner, L. Edelstein-Keshet, L. Bent, and A. Spiros. Mutual Interactions, Potentials, and Individual Distance in a Social Aggregation. *Journal of Mathematical Biology*, 47:353–389, 2003.
- [10] J.D. Murray. *Mathematical Biology I: An Introduction*. Springer, 2004.
- [11] D. Ruelle. *Statistical Mechanics: Rigorous Results*. W.A. Benjamin, New York, 1969.
- [12] C. Topaz, A. Bernoff, S. Logan, and W. Toolson. A Model for Rolling Swarms of Locusts. *European Physical Journal: Special Topics*, 157.1:93–109, 2008.
- [13] C. Topaz and A. Bertozzi. Swarming Patterns in a Two-Dimensional Kinematic Model for Biological Groups. *SIAM Journal of Applied Mathematics*, 65:152–174, 2004.
- [14] C. Topaz, A. Bertozzi, and M. Lewis. A Nonlocal Continuum Model for Biological Aggregation. *Bulletin of Mathematical Biology*, 2006.
- [15] T. Witelski and A. Bernoff. Self-Similar Asymptotics for Linear and Nonlinear Diffusion Equations. *Studies in Applied Mathematics*, 100:153–193, 1998.